

**An Analysis of Finite Elements for Plate
Bending Problems**

by

Alexander G. Iosilevich

Moscow State Technical University, Russia (1994)

Submitted to the Department of Mechanical Engineering
in partial fulfillment of the requirements for the degree of

Master of Science in Mechanical Engineering

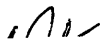
at the

MASSACHUSETTS INSTITUTE OF TECHNOLOGY

June 1996

© Massachusetts Institute of Technology 1996

All rights reserved



Signature of Author
Department of Mechanical Engineering
June 1996

Certified by
Klaus-Jürgen Bathe
Professor of Mechanical Engineering
~~Thesis~~ Supervisor

Accepted by
Ain Ants Sonin
Chairman, Graduate Committee

MASSACHUSETTS INSTITUTE
OF TECHNOLOGY

JUN 27 1996 Eng.

LIBRARIES

An Analysis of Finite Elements for Plate Bending Problems

by

Alexander G. Iosilevich

Submitted to the Department of Mechanical Engineering
on June 1996, in partial fulfillment of the
requirements for the degree of
Master of Science in Mechanical Engineering

Abstract

This thesis focuses on the inf-sup condition for Reissner-Mindlin plate bending finite elements. In general, one cannot analytically predict whether this fundamental condition for stability and optimality is satisfied for a given mixed finite element discretization. Therefore, we develop a numerical test methodology to tackle this issue, and apply the tests to the standard displacement-based elements and the elements of the MITC family. Whereas the pure displacement-based elements fail the tests, we find that the MITC elements pass them, which underlines the reliability of these elements for use in engineering practice.

Thesis Supervisor: Klaus-Jürgen Bathe
Title: Professor of Mechanical Engineering

Acknowledgements

I would like to express my sincere gratitude to my advisor, Professor Klaus-Jürgen Bathe, for his invaluable guidance, enthusiasm, and encouragement through the course of this work.

I am also indebted to Professor Valery Svetlitsky and Professor Alexander Gousskov from Moscow State Technical University, who introduced me to the field of Applied Mechanics.

In addition, it is my pleasure to thank my colleagues in the Finite Element Research Group at M.I.T., for their friendly support, invaluable discussions, and suggestions through the course of the research.

I would also like to thank ADINA R&D, Inc. for allowing me to use their proprietary software – ADINA, ADINA-IN, and ADINA-PLOT – during my work on this project.

Contents

| | | |
|----------|--|-----------|
| 1 | Introduction. | 9 |
| 1.1 | Overview. | 9 |
| 1.2 | Thesis outline. | 11 |
| 2 | Basic notions. | 12 |
| 2.1 | Mathematical background. | 12 |
| 2.1.1 | Assumptions on the domain. | 12 |
| 2.1.2 | Functional spaces. | 14 |
| 2.1.3 | A simple example. | 17 |
| 2.2 | The problem statement and mathematical models. | 19 |
| 2.3 | RM plate bending model. | 21 |
| 2.3.1 | Governing equations. Variational form. | 21 |
| 2.3.2 | Discrete variational problem. | 23 |
| 2.3.3 | Modified variational problem. | 26 |
| 2.4 | Mixed interpolation. FEM with Lagrange multipliers. | 26 |
| 2.4.1 | Limit problem. | 26 |
| 2.4.2 | Optimality in Γ' | 28 |
| 2.4.3 | Existence and uniqueness of the solution for FEM with Lagrange multipliers. | 31 |
| 3 | MITC plate bending elements. | 37 |
| 3.1 | Design principles. | 37 |

| | | |
|----------|--|-----------|
| 3.1.1 | Preliminary considerations. | 37 |
| 3.1.2 | Stokes analogy. | 39 |
| 3.1.3 | Construction of the elements. | 42 |
| 3.1.4 | Justification. | 44 |
| 3.2 | The elements. | 46 |
| 3.2.1 | Reference element and covariant transformation. | 46 |
| 3.2.2 | Displacement-based finite elements. | 47 |
| 3.2.3 | MITC4 element. | 48 |
| 3.2.4 | MITC9 element. | 50 |
| 3.2.5 | Other elements. | 52 |
| 4 | Numerical analysis. | 53 |
| 4.1 | Matrix computations. | 53 |
| 4.1.1 | Eigenvalue decompositions. Generalized eigenvalue problems. | 54 |
| 4.1.2 | Vector and matrix norms. Basic inequalities. | 55 |
| 4.2 | Analysis of the inf-sup condition. | 57 |
| 4.2.1 | Matrix form of the inf-sup condition in the Γ'_h -norm. | 57 |
| 4.2.2 | Discrete inf-sup condition in the L^2 -norm. | 58 |
| 4.2.3 | Inf-sup test in the Γ'_h -norm. | 60 |
| 4.2.4 | From Γ'_h to Γ' | 62 |
| 4.3 | Numerical results. | 67 |
| 5 | Conclusions. | 74 |
| A | Shear locking. | 76 |
| A.1 | Cantilever plate under a uniform load. | 76 |
| A.2 | Clamped square plate under a uniform load. | 79 |
| B | Inf-sup test in the Γ'_h-norm. | 83 |

List of Figures

- 2-1 (A) - Domain with Lipschitz-continuous boundary; (B) - Lipschitz-continuity is violated in the circled region. 13
- 2-2 Displacement assumptions of the RM plate bending model. 21
- 2-3 (A) - the saddle-point problem; (B) - contour plot of the saddle surface. 33
- 3-1 Surjective function. 45
- 3-2 Covariant transformation of a general element. 47
- 3-3 Tying procedure for the MITC4 element. 50
- 4-1 Cantilever plate considered in the inf-sup test. Top view shows a typical mesh of four none-node elements. 59
- 4-2 Inf-sup test of plate bending elements in the L^2 -norm (cantilever plate). 60
- 4-3 Inf-sup test of the plate elements in the Γ'_h -norm (cantilever plate). 62
- 4-4 Behavior of δ_n for quadrilateral plate bending elements (cantilever plate). 66
- 4-5 Clamped plate. 68
- 4-6 Uniform meshes used for the inf-sup test of the clamped plate case. 69
- 4-7 Inf-sup test of the quadrilateral plate bending elements in the Γ'_h -norm (clamped plate case, uniform meshes). 70

| | | |
|------|---|----|
| 4-8 | δ_n -test of the quadrilateral plate bending elements (clamped plate case, uniform meshes). | 71 |
| 4-9 | Distorted meshes used for the inf-sup test of the clamped plate problem. | 72 |
| 4-10 | Inf-sup test of the quadrilateral plate bending elements in the Γ'_h -norm (clamped plate, distorted meshes). | 73 |
| A-1 | Cantilever plate under a uniform load. | 76 |
| A-2 | Finite element solution (four-element meshes) for the cantilever plate case. (A) - transverse displacement w , mm ; (B) - rotation angle θ_y ; (C) - normal stress σ_{11} , MPa ; (D) - shear stress σ_{13} , MPa | 78 |
| A-3 | Clamped plate under a uniform load. | 79 |
| A-4 | FE solution for the transverse displacement w , mm , (8-by-8 uniform meshes for 4-node elements, 4-by-4 meshes for 9-node elements) for the clamped plate case. (A) - QUAD4 element; (B) - MITC4 element; (C) - QUAD9 element; and (D) - MITC9 element. | 81 |
| A-5 | FE solution for the transverse displacement w , mm , (8-by-8 distorted meshes for 4-node elements, 4-by-4 meshes for 9-node elements) for the clamped plate. (A) - QUAD4 element; (B) - MITC4 element; (C) - QUAD9 element; and (D) - MITC9 element. | 82 |

List of Tables

- A.1 Comparison of elements' performance in the norm $\|w_h\|$ (cantilever plate). 77
- A.2 Comparison of elements' performance in the norm $\|w_h\|$ (clamped plate case, uniform meshes, 8×8 meshes for four-node elements, 4×4 meshes for nine-node elements). 80
- A.3 Comparison of elements' performance in the norm $\|w_h\|$ (clamped plate case, uniform meshes, 16×16 meshes for four-node elements, 8×8 meshes for nine-node elements). 80
- A.4 Comparison of elements' performance in the norm $\|w_h\|$ (clamped plate case, distorted meshes, 8×8 meshes for four-node elements, 4×4 meshes for nine-node elements). 80
- A.5 Comparison of elements' performance in the norm $\|w_h\|$ (clamped plate case, distorted meshes, 16×16 meshes for four-node elements, 8×8 meshes for nine-node elements). 82

Chapter 1

Introduction.

1.1 Overview.

Finite element analysis of engineering problems in solid body mechanics often requires the use of plate bending elements. The design of such elements can be based on the Kirchhoff theory of plates. Then, because of the assumptions in this theory, the conforming finite element spaces are required to satisfy C^1 -continuity.

In the 1960's many Kirchhoff-theory-based conforming finite elements were proposed, among them the Clough and Tocher four-node quadrilateral element [21], the quadrilateral element based on the use of Hermitian functions by Bogner et al. [12], etc. Conforming plate elements were not only difficult to obtain, but also, the lower order elements turned out to be too stiff, resulting in displacements much less than the theoretical values. There were several attempts to use non-conforming elements, such as the nine-dof triangular element proposed by Bazeley et al. [11], but these elements often failed the patch test and even converged to incorrect results.

The subsequent research followed several different paths. Some researchers implemented elements based on alternative variational principles. One choice was to use the principle of complementary potential energy, which gave rise to

so-called "equilibrium formulations" ([51], [37]). These methods partly suffered from non-uniqueness of displacement fields, which were obtained from integrating the strains.

Another popular approach, known as the hybrid stress method, was pioneered by Pian and Tong ([40]). It is based on the use of Lagrange multipliers, which force interelement equilibrium in a modified principle of complementary potential energy.

Later Tong [50] developed the displacement hybrid approach, based on a modified form of the principle of minimum potential energy.

In the 1970's the first elements appeared built on the basis of Mindlin plate theory and reduced integration schemes. The motivation for the use of Mindlin theory was that only C^0 -continuity of the shape functions is required. As well, the simple shape functions from plane elasticity could be used along with isoparametric maps of distorted elements. This approach worked quite well for thick plates. However, as the thickness is decreased, the shear terms grow rapidly, in the limit resulting in zero displacements. This phenomenon was named (shear) locking.

To avoid shear locking, it becomes necessary either to impose the Kirchhoff compatibility condition directly as a constraint at discrete points or in the integral sense, or use some kind of numerical tricks (such as reduced integration) to avoid the unbounded growth of the shear energy part.

The latter direction was developed quite intensively in the 1970's ([53], [39]), while it was not realized that the use of reduced integration often distorts the results, and is not reliable to use in engineering practice.

The application of Lagrange multipliers to impose the Kirchhoff constraint resulted in the development of mixed methods. These element families, if properly designed, have a strong mathematical basis (see, e.g., [18] and references therein) and are robust to changes in thickness.

Of course, this brief review does not pretend to cover all directions and trends

in the plate bending element design and research. In particular, we have not mentioned "generalized equilibrium methods", "generalized displacement methods", and many others. For a much broader discussion we refer to the 1984 review article by Hrabok and Hrudey ([27]).

1.2 Thesis outline.

In Chapter 2 we start by covering some basic mathematical notions, which are abundantly used in the analysis of the finite element method. We define in a quite rigorous way the assumptions made, terminology used, and cite some general results dealing with associated functional spaces. Then we briefly cover existing mathematical models of the plate bending problem, and emphasize the basic assumptions and equations of the Reissner-Mindlin model. Finally we derive the mixed variational principle and show the necessary and sufficient conditions for existence, uniqueness, and stability of the solution.

Chapter 3 presents design principles and a mathematical analysis of the elements from the MITC (mixed interpolated tensorial components) family, and specifies the conditions reviewed in the second chapter for the problem under consideration.

Chapter 4 deals with numerical analysis of the elements, and provides the essential theory for tackling problems of the inf-sup type. There we develop a testing methodology, which allows to quantitatively analyze elements' "addiction" to locking behavior, and we apply these tests to the MITC elements and displacement-based elements.

Finally, Chapter 5 draws some conclusions and outlines possible extensions for further research.

Chapter 2

Basic notions.

2.1 Mathematical background.

This section summarizes some mathematical notions and definitions which are extensively used in the mathematical analysis of the finite element method (FEM).

2.1.1 Assumptions on the domain.

The problem of consideration is posed in the domain $\Omega \in \mathbb{R}^n$, $n = 2$, with sufficiently smooth boundary $\partial\Omega$. Let us formally define what is usually meant by the "sufficiently smooth boundary" ([22]) in the finite element literature.

An open set $\Omega \in \mathbb{R}^n$ has a Lipschitz-continuous boundary if there exist constants $\alpha, \beta > 0$, a number of local reference coordinate systems $\{\underline{Q}_r^j \in \mathbb{R}^n, \underline{x}_r^j\}$ and local maps $a^j(\cdot)$, $j = 1..J$, Lipschitz-continuous¹ on their respective domains

¹A real-valued function f of a single real variable x , defined over a domain Ω is Lipschitz-continuous if:

$$|f(x_1) - f(x_2)| \leq C|x_1 - x_2| \quad \forall (x_1, x_2) \in \Omega,$$

where C is known as the Lipschitz constant.

of definition $\{\underline{x}_r^j \in \mathbb{R}^{n-1} : |\underline{x}_r^j| \leq \alpha\}$, such that

$$\partial\Omega = \bigcup_{j=1}^J \{x^j : x^j = a^j(\underline{x}_r^j), |\underline{x}_r^j| < \alpha\},$$

$$\{x^j : a^j(\underline{x}_r^j) < x^j < a^j(\underline{x}_r^j) + \beta, |\underline{x}_r^j| < \alpha\} \in \Omega,$$

$$\{x^j : a^j(\underline{x}_r^j) - \beta < x^j < a^j(\underline{x}_r^j), |\underline{x}_r^j| < \alpha\} \in \bar{\Omega},$$

where $\bar{\Omega}$ stands for the complement of Ω , ($\bar{\Omega} = \mathbb{R}^n \setminus \Omega$).

Geometrical interpretation of this condition for $\Omega \in \mathbb{R}^2$ is shown in Fig. 2-1.

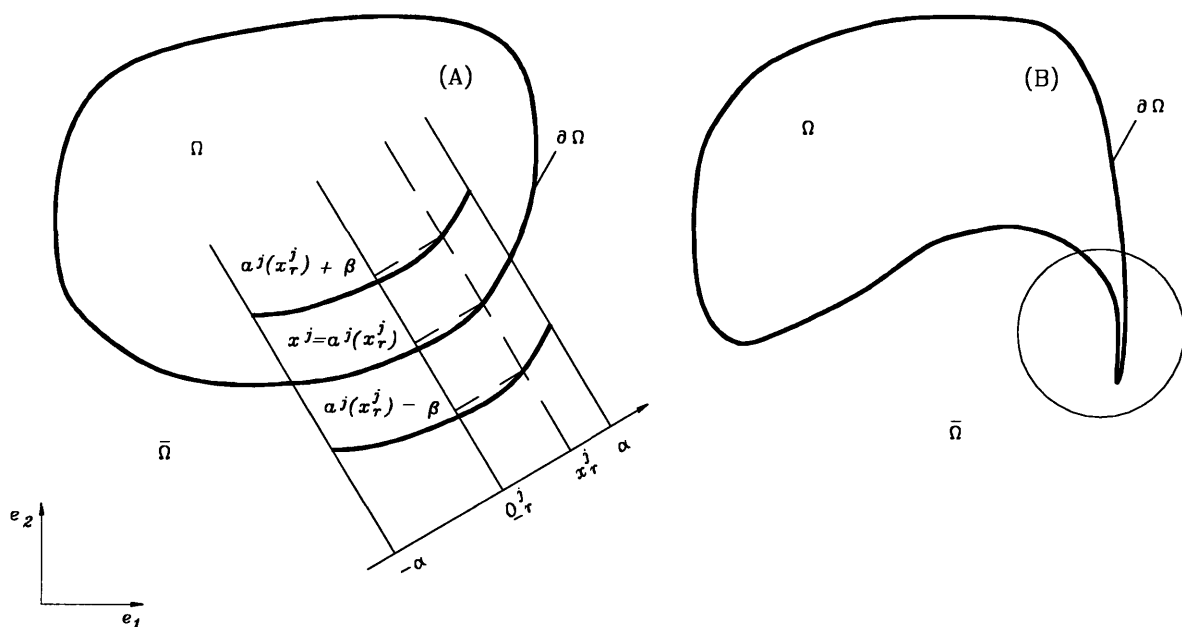


Figure 2-1: (A) - Domain with Lipschitz-continuous boundary; (B) - Lipschitz-continuity is violated in the circled region.

The definition above allows to consider all commonly encountered shapes, though eliminating some special cases, such as domains with cusped corners, cracks, etc., which require special treatments (see e.g. Chap. 8 of [46]).

When all of the maps $a^j(\cdot)$, $j = 1..J$ are linear, we have a special case, that is, Ω is a *convex polygon*.

If an open set Ω is connected and there exists a finite number of convex polygons Ω_k , such that $\Omega = \overline{\left(\bigcap_{k=1}^K \overline{\Omega}_k\right)}$, then Ω is called a *polygon*.

We will always assume that one of the following properties hold:

- Ω has a Lipschitz-continuous boundary; or
- Ω is a polygon.

In either case Ω is *bounded*, that is, there exists a constant $M : \|\underline{v}\| \leq M \quad \forall \underline{v} \in \Omega$ (in other words, any vector drawn inside Ω has a finite length – i.e., semiinfinite bodies that often appear in the elasticity do not satisfy this condition).

2.1.2 Functional spaces.

In this section we introduce the basic functional spaces that will enable us to make variational statements.

A real-valued function f is said to be *Lebesgue measurable* on Ω if for every real number λ , the subset $\omega : f|_{\omega} > \lambda$ is measurable².

Firstly, for $L^p(\Omega)$, $p \in [1, \infty)$, we set

$$L^p(\Omega) = \left\{ v \in \mathcal{M}(\Omega) \mid \int_{\Omega} |v|^p d\Omega < \infty \right\}, \quad \|v\|_{L^p(\Omega)} = \left(\int_{\Omega} |v|^p d\Omega \right)^{\frac{1}{p}}, \quad (2.1)$$

where $\mathcal{M}(\Omega)$ stands for the space of functions, Lebesgue measurable over domain Ω .

² $f(x) = \frac{1}{x}$ is an example of a function measurable on the interval $\Omega = [-1; 1]$. Although $f(x)$ is not bounded on the subset $\omega = \{x = 0\}$, the measure (length) of ω certainly is well-defined, and equals to zero. Examples of nonmeasurable functions are more difficult to find, although they certainly exist (see, i.e., [30]).

Remark. All finite element spaces are constructed over the space $\mathcal{M}(\Omega)$. This guarantees that integrals of the functions under consideration are well-defined, or, roughly speaking, functions are not too irregular (i.e., functions that have infinitely many singularities are not admissible). For example, such cases as an infinite stress in the semiinfinite body are ruled out by construction. \square

In future, we will deal with one particular member of the family, namely, the space of square-integrable functions, $L^2(\Omega)$, with the scalar product given by

$$(u, v)_{L^2(\Omega)} = \int_{\Omega} uv \, d\Omega.$$

The operation (\cdot, \cdot) would be considered as the $L^2(\Omega)$ -inner product by default.

Secondly, we introduce the Hilbertian Sobolev spaces (in future referred to simply as Sobolev spaces) with an integer index $H^k(\Omega)$:

$$H^k(\Omega) = \left\{ v \in L^2(\Omega), D^\alpha v \in L^2(\Omega), |\alpha| \leq k \right\},$$

where

$$D^\alpha v = \frac{\partial^{|\alpha|} v}{\partial x_1^{\alpha_1} \dots \partial x_n^{\alpha_n}}, \quad |\alpha| = \sum_{i=1}^n \alpha_i;$$

equipped with the following inner product, seminorm, and norm:

$$(u, v)_{H^k(\Omega)} = \int_{\Omega} \sum_{|\alpha|=0}^k D^\alpha u D^\alpha v \, d\Omega,$$

$$|v|_{H^k(\Omega)} = \left(\sum_{|\alpha|=k} \|D^\alpha v\|_{L^2(\Omega)}^2 \right)^{\frac{1}{2}}, \quad \|v\|_{H^k(\Omega)} = \left(\sum_{|\alpha|=0}^k \|D^\alpha v\|_{L^2(\Omega)}^2 \right)^{\frac{1}{2}}.$$

The following inequality holds. *Let a real valued function $f(x_1, \dots, x_n) \in H^k(\Omega)$, with $k > n/2$, and let f be continuous, then*

$$\max |f| \leq C \|f\|_{H^k(\Omega)}. \quad (2.2)$$

This inequality is often referred to as *Sobolev inequality*.

Example.

To demonstrate the implications of the inequality (2.2), consider a function

$$f(x, y) = f(r) = \lg(\lg(r)),$$

defined over a domain $\Omega = \left\{r, r = \sqrt{x_1^2 + x_2^2} \mid r \leq 1/2\right\}$. One can show that $f \in H^1(\Omega)$, i.e., $\|f\|_{H^1(\Omega)} < C_1 < \infty$. Therefore, we have $k = n/2 = 1$, and the Sobolev rule says that we would be unable to identify an upper bound for f on Ω . Indeed, we have that $f \xrightarrow{r \rightarrow 0} \infty$, and the inequality (2.2) clearly does not hold.

□

The family of functional spaces defined below corresponds to the homogeneous boundary conditions on $\partial\Omega$ (homogeneous spaces)

$$H_0^k(\Omega) = \left\{v \in H^k(\Omega), D^\alpha v|_{\partial\Omega} = 0, |\alpha| \leq k-1\right\}.$$

When the domain Ω is bounded, we have the following norm equivalence, referred to as *Poincaré-Friedrichs inequality* [22]:

$$c_0(\Omega) \|v\|_{H^k(\Omega)} \leq |v|_{H_0^k(\Omega)} \leq c_1(\Omega) \|v\|_{H^k(\Omega)} \quad (2.3)$$

For the further analysis we also need spaces of functionals $\mathcal{L} : H^k(\Omega) \rightarrow \mathbb{R}$, defined over the Sobolev spaces (topological duals, or so called *negative Sobolev spaces*): $H^{-k}(\Omega) \equiv (H^k(\Omega))'$. For a pair $(f, u) : u \in \mathcal{K}, f \in \mathcal{K}'$, where \mathcal{K} stands for a Sobolev space, we define a *duality pairing* on $\mathcal{K}' \times \mathcal{K}$ (a map $: \mathcal{K}' \times \mathcal{K} \rightarrow \mathbb{R}$) as:

$$f(u) \equiv \langle f, u \rangle_{\mathcal{K}' \times \mathcal{K}}.$$

The corresponding dual norm is

$$\|f\|_{\mathcal{K}'} = \sup_{u \in \mathcal{K}, u \neq 0} \frac{|\langle f, u \rangle_{\mathcal{K}' \times \mathcal{K}}|}{\|u\|_{\mathcal{K}}}.$$

The following result is referred to as *the Riesz Representation Theorem*:

Let \mathcal{K} be a Hilbert space, and $f \in \mathcal{K}'$ be a continuous linear functional on \mathcal{K} . Then there exist a unique $u_0 \in \mathcal{K}$, such that $f(u) = (u_0, u)_{\mathcal{K}}$, $\forall u \in \mathcal{K}$.

Moreover, $\|f\|_{\mathcal{K}'} = \|u_0\|_{\mathcal{K}}$.

The proof of the theorem can be found, e.g., in [38], [52].

In case $\Omega = \{x : x \in]x_1; x_2[\subset \mathbb{R}\}$, we have the following mapping K [38], $K : H^k(\Omega) \rightarrow H^{-k}(\Omega)$,

$$K = \sum_{m=0}^k (-1)^m \frac{d^{2m}}{dx^{2m}}. \quad (2.4)$$

Finally, we state the following *inclusion property* of the Sobolev spaces

$$H^m(\Omega) \subset H^{m-1}(\Omega) \subset \dots \subset H^0(\Omega) \subset \dots \subset H^{-m+1}(\Omega) \subset H^{-m}(\Omega), \quad \forall m > 0. \quad (2.5)$$

For a general study of the Sobolev spaces we refer to [1].

2.1.3 A simple example.

Consider a truss of length L ($\Omega = \{x : x \in]0; L[\}$) fixed at the end points $x = 0$, $x = L$, under the action of a distributed load $f(x)$. Let the deflection of the truss be $w(x) : w(x) \in H_0^1(\Omega)$ (clearly, this must be the case of a real physical system), and presume that f is square-integrable over Ω . Noting that $f(x) \in L^2(\Omega) \xrightarrow{\text{by (2.5)}} f(x) \in H^{-1}(\Omega) = (H^1(\Omega))'$, we can define a duality pairing as

$$\langle f, w \rangle_{H^{-1}(\Omega) \times H^1(\Omega)} = \int_0^L f w \, dx, \quad (2.6)$$

which has a meaning of the work done by external forces. Actually, to obtain a finite number as a result of the duality, we do not have to enforce w to be in H^1 ; indeed, the L^2 regularity is sufficient for the functional in (2.6) to make sense (to give a finite number).

Now we consider the case $f(x) = \delta(x - L/2)$, that is $f(x) \in H^{-1}(\Omega)$. In this case, to obtain a finite scalar number after the integration, $w(x)$ must be continuous on Ω ; we have to use the fact that $w(x) \in H_0^1(\Omega)$, and the duality pairing defined above still works.

The norm of f can be calculated as

$$\|f\|_{H^{-1}(\Omega)} = \max_{v \in H^1(\Omega)} \frac{v(L/2)}{\|v\|_{H^1(\Omega)}} \stackrel{\text{by (2.2)}}{<} C,$$

which is finite, according to Sobolev's inequality.

To demonstrate a Riesz representation of $f(x)$ in $H_0^1(\Omega)$, we will find a linear operator K , such that every $v(x) \in H_0^1(\Omega)$ has a unique image $Kv(x)$ in $H^{-1}(\Omega)$. Using formula (2.4), we can simply construct this operator as $K = -\frac{d^2}{dx_2} + 1$. Since $H^{-1}(\Omega)$ contains $H_0^1(\Omega)$ as well as singular functions of type $f(x)$, the operator K can be understood as a superposition of δ -function-like distributions, given by the first term, and $H_0^1(\Omega)$ represented by the unitary transformation. To find an element $v_f(x) \in H_0^1(\Omega)$ that is the Riesz representation of f , we have to solve a differential equation

$$Kv_f(x) = -\frac{d^2v_f(x)}{dx_2} + v_f(x) = f(x).$$

The solution is $v_f(x) = -H(x - L/2) \sinh(x - L/2) + \frac{\sinh(-L/2) \sinh(x)}{\sinh(-L)}$. Recalling that the inner product in $H^1(\Omega)$ is given by $(u, v)_{H^1(\Omega)} = \int_0^L \left(uv + \frac{du}{dx} \frac{dv}{dx} \right) dx$,

one can check that indeed,

$$\int_0^L fw \, dx = w(L/2) = (v_f, w)_{H^1(\Omega)} \quad \forall w \in H_0^1(\Omega). \quad \square$$

2.2 The problem statement and mathematical models.

Consider a three-dimensional linear elastic body \mathcal{B} that, in the absence of external loading, occupies the region

$$\mathcal{D} = \left\{ \underline{x} = (x_1, x_2, x_3) \in \mathbb{R}^3 \mid (x_1, x_2) \in \Omega, x_3 \in \left[-\frac{t}{2}, \frac{t}{2}\right] \right\},$$

where $\Omega \in \mathbb{R}^2$ is a bounded smooth domain with boundary $\partial\Omega$, and $t > 0$ is "relatively small" with respect to $\text{diam}(\Omega)$.

By the *exact solution of a linear elastic plate bending problem*, we understand the solution of the three-dimensional linear elasticity problem of deformation of the body \mathcal{B} under the action of a transverse load $\underline{f} = (0, 0, f_3(x_1, x_2))$. The further analysis is restricted to the case of isotropic homogeneous material with elastic constants E and ν , being the modulus of elasticity and Poisson's ratio, respectively. Denoting $\underline{u} = \{u_i\}$, $\underline{\sigma} = \{\sigma_{ij}\}$, and $\underline{\varepsilon} = \{\varepsilon_{ij}\}$, $i, j = 1..3$, as the displacement vector, stress tensor, and strain tensor, respectively, we have the following stress-strain relations given by Hooke's law:

$$\begin{bmatrix} \sigma_{11} \\ \sigma_{22} \\ \sigma_{33} \\ \sigma_{12} \\ \sigma_{23} \\ \sigma_{13} \end{bmatrix} = \begin{bmatrix} \lambda + 2\mu & \lambda & \lambda & & & \\ & \lambda & \lambda + 2\mu & & & \\ & \lambda & \lambda & \lambda + 2\mu & & \\ & & & & 2\mu & \\ & & & & & 2\mu \\ & & & & & & 2\mu \end{bmatrix} \begin{bmatrix} \varepsilon_{11} \\ \varepsilon_{22} \\ \varepsilon_{33} \\ \varepsilon_{12} \\ \varepsilon_{23} \\ \varepsilon_{13} \end{bmatrix},$$

where $\lambda = \frac{E\nu}{(1+\nu)(1-2\nu)}$ and $\mu = \frac{E}{2(1+\nu)}$ are the Lamé constants (elements not shown are zeroes).

By the *plate bending model* we mean a two-dimensional boundary value problem with a solution, which approximates the exact solution of the plate bending problem.

The following two models are extensively used in engineering practice (see [26], [3] for the comparison of the models and references therein):

- *The Kirchhoff model* (see, e.g., [48]) is based on the assumption that all out-of-plane components of the stress tensor are negligible (we set the components σ_{i3} , $i = 1..3$, to be zero). Geometrically this implies that a straight element normal to the midsurface remains straight and normal after deformations. This model provides a good approximation for the plate bending problem only for thin plates, that is, in the case $t \ll \text{diam}(\Omega)$. The most important disadvantage of the model is that the strains are calculated as corresponding second derivatives of the state variable w (transverse displacement). In terms of finite elements, it requires C^1 continuity of the interpolation functions. Moreover, the model suffers from the inherent limitations, such as paradoxical artificial reaction forces on the corners of polygonal domains, and difficulties in imposing natural boundary conditions.
- *The Reissner-Mindlin model (RM)* ([43], [36]) uses the condition $\sigma_{33} \ll \sigma_{11}, \sigma_{22}$ (that is, we set only σ_{33} to be zero, leaving shear strains for the consideration), and therefore, is closer to the original 3D problem. The basic hypothesis of this model is that a straight line normal to the undeformed plate surface Ω remains straight but not necessarily normal during the deformation (see Fig. 2-2). Finite elements based on this RM model need to have only C^0 continuity of the interpolating spaces. Moreover, this approach is far more flexible in allowing to model many types of boundary conditions without significant difficulties (see [26]).

2.3 RM plate bending model.

This section describes the basic equations and specific difficulties associated with the RM plate bending model. The more precise analysis can be found in [48] and [23].

2.3.1 Governing equations. Variational form.

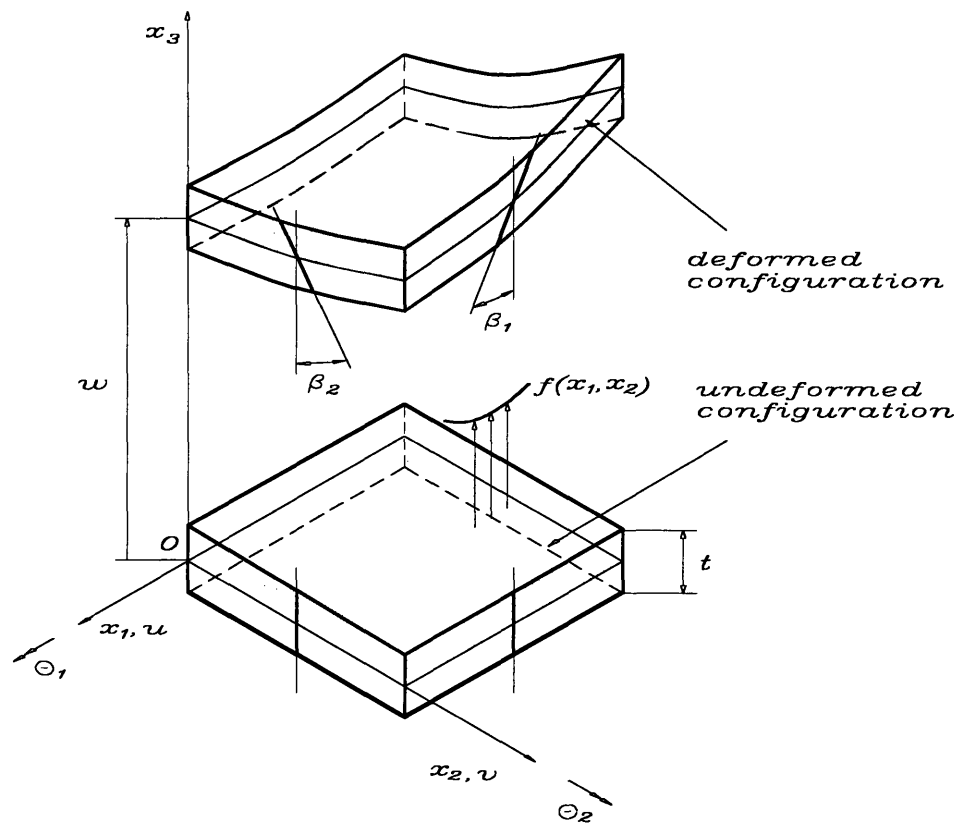


Figure 2-2: Displacement assumptions of the RM plate bending model.

The equations governing the model are [6]:

1. Displacements (assumed to be small)

$$u_1 = -x_3\beta_1; \quad u_2 = -x_3\beta_2; \quad u_3 = w, \quad (2.7)$$

where β_1, β_2 , and w are the scalar functions of the in-plane vector coordinate $\underline{x} = (x_1, x_2)$.

2. Strains (linear part of the strain tensor)

$$\begin{aligned} \varepsilon_{11} &= -x_3\beta_{1,1}; & \varepsilon_{22} &= -x_3\beta_{2,2}; & \varepsilon_{12} &= -\frac{1}{2}x_3(\beta_{1,2} + \beta_{2,1}); \\ \varepsilon_{13} &= \frac{1}{2}(w_{,1} - \beta_1); & \varepsilon_{23} &= \frac{1}{2}(w_{,2} - \beta_2), \end{aligned} \quad (2.8)$$

where " $F_{,i}$ " denotes the partial derivative $\frac{\partial F}{\partial x_i}$.

3. Stresses (isotropic elastic material assumption)

$$\begin{aligned} \sigma_{11} &= \frac{E}{1-\nu^2}(\varepsilon_{11} + \nu\varepsilon_{22}); & \sigma_{22} &= \frac{E}{1-\nu^2}(\varepsilon_{22} + \nu\varepsilon_{11}); & \sigma_{33} &\equiv 0; \\ \sigma_{12} &= 2G\varepsilon_{12}; & \sigma_{13} &= 2G\varepsilon_{13}; & \sigma_{23} &= 2G\varepsilon_{23}, \end{aligned} \quad (2.9)$$

where G stands for the shear modulus, $G = \frac{E}{2(1+\nu)}$.

4. The variational form as a starting point for a finite element analysis is formulated within the principle of minimal potential energy [28]. For the case of a clamped plate (the treatment of other types of boundary conditions is also possible, see [26]), we have the following *minimization problem*

$$\begin{aligned} \text{Find } \underline{u} &= (\underline{\beta}, w) \in V = B \times W = [H_0^1(\Omega)]^2 \times H_0^1(\Omega) \text{ such that} \\ \underline{u} &= \arg \min_{\underline{v}=(\underline{\eta}, \xi) \in V} \left\{ \frac{1}{2} \left[a(\underline{\eta}, \underline{\eta}) + \frac{Gk}{t^2} (\nabla \xi - \underline{\eta}, \nabla \xi - \underline{\eta}) \right] - \frac{1}{t^3} (f, \xi) \right\} = \\ &= \arg \min_{\underline{v}=(\underline{\eta}, \xi) \in V} \left\{ \frac{1}{2} \mathcal{A}(\underline{v}, \underline{v}) - \frac{1}{t^3} (f, \xi) \right\}, \end{aligned} \quad (2.10)$$

where $a(\cdot, \cdot)$ is a symmetric bilinear form defined as

$$a(\underline{\eta}_1, \underline{\eta}_2) = \frac{D}{t^3} \int_{\Omega} [(1 - \nu) \underline{\underline{\varepsilon}}(\underline{\eta}_1) \cdot \underline{\underline{\varepsilon}}(\underline{\eta}_2) + \nu (\nabla \cdot \underline{\eta}_1) (\nabla \cdot \underline{\eta}_2)] d\Omega;$$

$\underline{\underline{\varepsilon}}(\underline{\eta})$ is the linear strain operator:

$$\underline{\underline{\varepsilon}}(\underline{\eta}) = \eta_{1,1} \underline{e}_1 \underline{e}_1 + \eta_{1,2} \underline{e}_1 \underline{e}_2 + \eta_{2,1} \underline{e}_2 \underline{e}_1 + \eta_{2,2} \underline{e}_2 \underline{e}_2;$$

$$\nabla = \frac{\partial}{\partial x_1} \underline{e}_1 + \frac{\partial}{\partial x_2} \underline{e}_2;$$

(\cdot, \cdot) is the $L^2(\Omega)$ -inner product;

$D = \frac{Et^3}{12(1 - \nu^2)}$ stands for the flexural rigidity of the plate; and

k is the shear correction factor that accounts for the nonuniformity of the shear strain distribution through the plate thickness, usually $k = 5/6$.

Note that for a finite fixed thickness t we have, expanding the bilinear forms and collecting the corresponding terms,

$$\mathcal{A}(\underline{v}, \underline{v}) = a(\underline{\eta}, \underline{\eta}) + \frac{Gk}{t^2} (\nabla \xi - \underline{\eta}, \nabla \xi - \underline{\eta}) \geq C \|\underline{v}\|_1 = C (\|\underline{\eta}\|_1 + \|\xi\|_1), \quad (2.11)$$

that is, $\mathcal{A}(\underline{v}, \underline{v})$ is an elliptic bilinear form (the constant C in the inequality above depends on thickness and material properties of the plate).

The minimization problem (2.10) can be equivalently represented in the *variational form*:

$$\text{Find } \underline{u} = (\underline{\beta}, w) \in V = B \times W = [H_0^1(\Omega)]^2 \times H_0^1(\Omega) \text{ such that} \quad (2.12)$$

$$a(\underline{\beta}, \underline{\eta}) + \frac{Gk}{t^2} (\nabla w - \underline{\beta}, \nabla \xi - \underline{\eta}) = \frac{1}{t^3} (f, \xi) \quad \forall \underline{v} = (\underline{\eta}, \xi) \in V,$$

2.3.2 Discrete variational problem.

Typically one cannot find an analytical solution to (2.12). The usual way to proceed is to introduce a finite-dimensional problem which approximates the given one.

Let us choose a discrete space $V_h = B_h \times W_h \subset V$, where $B_h \subset B$, and $W_h \subset W$; thus we are restricted to using a *conforming approximation*.

Following the *Rayleigh-Ritz procedure*, we obtain the corresponding discrete minimization problem over the space V_h

$$\begin{aligned} \text{Find } \underline{u}_h &= (\underline{\beta}_h, w_h) \in V_h = B_h \times W_h, \text{ such that} \\ \underline{u}_h &= \arg \min_{\underline{v}_h = (\underline{\eta}_h, \xi_h) \in V_h} \left\{ \frac{1}{2} \mathcal{A}(\underline{v}_h, \underline{v}_h) - \frac{1}{t^3} (f, \xi_h) \right\}. \end{aligned} \quad (2.13)$$

Locking.

Let us rewrite the minimization problem (2.13) in the *discrete variational form*. For the following analysis, let us rescale the loading term f as $f = t^3 g$, with g independent of plate thickness t . Then in case of finite t we have the following *discrete variational problem*

$$\begin{aligned} \text{Find } \underline{u}_h &= (\underline{\beta}_h, w_h) \in V_h = B_h \times W_h, \text{ such that} \\ a(\underline{\beta}_h, \underline{\eta}_h) + \frac{Gk}{t^2} (\nabla w_h - \underline{\beta}_h, \nabla \xi_h - \underline{\eta}_h) &= (g, \xi_h) \quad \forall \underline{v}_h = (\underline{\eta}_h, \xi_h) \in V_h. \end{aligned}$$

As $t \rightarrow 0$, we have that $a(\underline{\beta}_h, \underline{\eta}_h) \sim 1$, $\frac{Gk}{t^2} \sim \frac{1}{t^2}$ with $\lim_{t \rightarrow 0} \frac{Gk}{t^2} = \infty$. Although the thickness may be very small, the energy of deformation still remains finite. To keep it finite, we must have that the shear strain contribution to the total potential vanishes, that is $(\nabla w_h - \underline{\beta}_h, \nabla \xi_h - \underline{\eta}_h) = 0$ for all $(\underline{\eta}_h, \xi_h) \in V_h$. Clearly, this is nothing else, but the integral form of the celebrated Kirchhoff constraint

$$\nabla w = \underline{\beta}. \quad (2.14)$$

Equation (2.14) implies that in the limit case, the RM model must degenerate to satisfy conditions on the stress-strain state, described by the Kirchhoff hypothesis. Thus, as we approach the limit case, the finite element solution is

more and more enforced to satisfy the Kirchhoff constraint. Consequently, the number of "conforming" (which can represent the Kirchhoff hypothesis (2.14)) trial functions in the discrete space V_h may get severely restricted, and this can result in partial or even total loss of convergence properties of the finite element approximation. This phenomenon is known in the literature as *(shear) locking* (see, e.g. [6], [47]).

Another difficulty for the numerical solution is due to the existence of boundary layers for various types of boundary conditions ([3], [44]).

General approaches.

There are two general approaches to circumvent the problem of locking described above. The first type of methods is based on the standard variational formulation, and uses convergence properties of higher order FE spaces (so-called *p-version* and certain higher-order *h-versions* [4]).

The other approach is to modify the variational formulation, and therefore, come to a different finite element formulation. The reasons for that treatment are:

- Difficulty to construct low-order finite element spaces, satisfying the constraint (2.14) exactly;
- Possibility to introduce variables that have a certain physical interpretation.

Those ideas are used in *mixed* and *hybrid* FEM (some other approaches, based on modifications of the variational form, such as *reduced integration* [35] and *penalty formulations* are also well known in the literature). For some examples of hybrid plate bending elements we refer to a recent paper [31], while some mixed finite elements would be the subject of the following discussion.

2.3.3 Modified variational problem.

The general guideline is to replace the Kirchhoff constraint by a weaker form, introducing a reduction operator R_h into the variational statement:

$$a(\underline{\beta}_h, \underline{\eta}_h) + \frac{Gk}{t^2} (R_h(\nabla w_h - \underline{\beta}_h), R_h(\nabla \xi_h - \underline{\eta}_h)) = (g, \xi_h) \quad (2.15)$$

Thus, choosing $R_h = I$, we have the standard FEM; if the reduction is based on inaccurate numerical quadratures in evaluating the shear strain energy, we in essence use the idea of *selective* or *reduced integration* (if we treat distorted elements by reduced integration, the operator R_h may become highly nonlinear, and could hardly be found in closed form). In the following, we will consider the case of *mixed interpolation*, where the shear stress is first approximated independently and then eliminated from the system.

Clearly, the choice of R_h in (2.15) is crucial: it should weaken the constraint (2.14) sufficiently, so that the FE spaces would retain their approximation properties, while on the other hand, it should not weaken it too much, since otherwise the consistency error may become too large (that is, our solution will be far from the real one), or even the solvability conditions may be violated.

2.4 Mixed interpolation. FEM with Lagrange multipliers.

2.4.1 Limit problem.

Before we proceed with mixed interpolation, let us define the shear stress in the plate and its discrete approximation as

$$\underline{\gamma} = \frac{Gk}{t^2} (\nabla w - \underline{\beta}), \quad \underline{\gamma}_h = \frac{Gk}{t^2} (\nabla w_h - \underline{\beta}_h). \quad (2.16)$$

Considering the variational problem (2.12), we note that for a finite thickness t , the fact that $\nabla w \in \nabla W \subseteq [L^2(\Omega)]^2$, $\nabla w_h \in \nabla W_h \subset \nabla W$, implies that both the shear stresses and their discrete version are sufficiently smooth ($\underline{\gamma} \in \mathcal{G} \subseteq [L^2(\Omega)]^2$, $\underline{\gamma}_h \in \mathcal{G}_h \subset \mathcal{G}$). Noting that all linear operators defined on $L^2(\Omega)$ are indeed in $L^2(\Omega)$ (that is, $[L^2(\Omega)]' = L^2(\Omega)$ ³), we can represent equation (2.16) in the integral form as

$$(\underline{\gamma}, \underline{\varepsilon}) = \left(\frac{Gk}{t^2} (\nabla w - \underline{\beta}), \underline{\varepsilon} \right) \quad \forall \underline{\varepsilon} \in \mathcal{G}.$$

This allows us to rewrite the variational problem (2.12) as

$$\begin{aligned} \text{Find } \underline{u} = (\underline{\beta}, w) \in V = B \times W = [H_0^1(\Omega)]^2 \times H_0^1(\Omega), \underline{\gamma} \in \mathcal{G}, \text{ such that} \\ \begin{cases} a(\underline{\beta}, \underline{\eta}) + (\underline{\gamma}, \nabla \xi - \underline{\eta}) = (g, \xi) & \forall \underline{v} = (\underline{\eta}, \xi) \in V, \\ \left(\frac{t^2}{Gk} \underline{\gamma} - (\nabla w - \underline{\beta}), \underline{\varepsilon} \right) = 0 & \forall \underline{\varepsilon} \in \mathcal{G}. \end{cases} \end{aligned} \quad (2.17)$$

However, as we approach the limit case, $t \rightarrow 0$, we lose the regularity of $\underline{\gamma}$ in the L^2 -norm, that is

$$\|\underline{\gamma}\|_{L^2(\Omega)} = \left[\int_{\Omega} (\underline{\gamma} \cdot \underline{\gamma}) \, d\Omega \right]^{1/2} = \frac{Gk}{t^2} \left[\int_{\Omega} (\nabla w - \underline{\beta})^2 \, d\Omega \right]^{1/2} \rightarrow \infty.$$

This suggests that we should look for the space for shears among the negative Sobolev spaces, as in the example in section (2.1.3), and the appropriate space \mathcal{K}' would be the smallest one, in which the corresponding norm is finite, that is

³Namely, consider a function $f \in [L^2(\Omega)]'$. We have

$$\begin{aligned} \|f\|_{[L^2(\Omega)]'} &= \sup_{v \in L^2(\Omega), v \neq 0} \frac{\langle f, v \rangle_{[L^2(\Omega)]' \times L^2(\Omega)}}{\|v\|_{L^2(\Omega)}} = \sup_{v \in L^2(\Omega), v \neq 0} \frac{\langle f, v \rangle}{\sqrt{(v, v)}} \\ &= \sqrt{(f, f)} = \|f\|_{L^2(\Omega)} \end{aligned}$$

therefore clearly, $f \in L^2(\Omega)$.

$\|\underline{\gamma}\|_{\mathcal{X}'} \leq c$. Ideally, the constant appearing on the r.h.s. of this inequality should not depend on the plate thickness t , though it is neither sufficient nor necessary for the bound to exist. In the following section we will show that the normed space $\Gamma' = H^{-1}(\text{div}; \Omega)$ satisfies the requirements given above, and

$$H^{-1}(\text{div}; \Omega) = \left\{ \underline{\gamma} \in [H^{-1}(\Omega)]^2, \nabla \cdot \underline{\gamma} \in H^{-1}(\Omega) \right\}, \quad (2.18)$$

$$\|\underline{\gamma}\|_{H^{-1}(\text{div}; \Omega)}^2 = \|\underline{\gamma}\|_{H^{-1}(\Omega)}^2 + \|\nabla \cdot \underline{\gamma}\|_{H^{-1}(\Omega)}^2$$

Therefore, when t approaches zero, we are able to pose the following *limit problem*:

$$\begin{aligned} \text{Find } \underline{u}^0 = (\underline{\beta}^0, w^0) \in V = B \times W = [H_0^1(\Omega)]^2 \times H_0^1(\Omega) \text{ and} \\ \underline{\gamma}^0 \in \Gamma' = H^{-1}(\text{div}; \Omega), \text{ such that} \end{aligned} \quad (2.19)$$

$$\begin{cases} a(\underline{\beta}^0, \underline{\eta}) + (\underline{\gamma}^0, \nabla \xi - \underline{\eta}) = (g, \xi) & \forall \underline{v} = (\underline{\eta}, \xi) \in V, \\ (\nabla w^0 - \underline{\beta}^0, \underline{\zeta}) = 0 & \forall \underline{\zeta} \in \Gamma' \end{cases}$$

2.4.2 Optimality in Γ' .

Here we cite the result from the original paper [7], which explicitly shows the optimality of the norm in $H^{-1}(\text{div}; \Omega)$ (optimality is obtained in the sense that the norm of the shears in that space is finite and bounded by a constant independent of the plate thickness).

Theorem 1. We have

$$\|\underline{\gamma}(t)\|_{H^{-1}(\text{div}; \Omega)} \leq c \text{ independent of } t. \quad (2.20)$$

Proof.

1. For a finite but small t we have the following bound for the solution of (2.17):

$$\|\underline{u}\|_V^2 + t^2 \|\underline{\gamma}(t)\|_{L^2(\Omega)}^2 \leq c \text{ independent of } t, \quad (2.21)$$

where $\|\underline{u}\|_V^2 = \|\underline{\beta}\|_{H^1(\Omega)}^2 + \|w\|_{H^1(\Omega)}^2$.

2. By the *Riesz Representation Theorem*, we have that there exists a unique $\underline{\chi} \in \Gamma$: $(\underline{\gamma}(t), \underline{\chi}) = \langle \underline{\gamma}, \underline{\chi} \rangle_{\Gamma' \times \Gamma} = \|\underline{\gamma}(t)\|_{\Gamma'}^2 = \|\underline{\chi}\|_{\Gamma}^2$, where

$$\begin{aligned} \Gamma &\equiv (\Gamma')' = [H^{-1}(\operatorname{div}; \Omega)]' = H_0(\operatorname{rot}; \Omega) = \\ &= \{ \underline{\chi} \in [L^2(\Omega)]^2, \operatorname{rot} \underline{\chi} \in L^2(\Omega), \underline{\chi} \cdot \underline{\tau} = 0 \text{ on } \partial\Omega \}, \end{aligned} \quad (2.22)$$

$$\|\underline{\chi}\|_{\Gamma} = \sup_{\underline{\gamma} \in \Gamma', \underline{\gamma} \neq 0} \frac{|\langle \underline{\chi}, \underline{\gamma} \rangle_{\Gamma' \times \Gamma}|}{\|\underline{\gamma}\|_{\Gamma'}}, \text{ where}$$

$$\operatorname{rot} : \underline{u} \rightarrow \operatorname{rot} \underline{u} = -\frac{\partial u_1}{\partial x_2} + \frac{\partial u_2}{\partial x_1}.$$

3. Choose $\underline{\theta} \in B$ such that

$$\nabla \cdot \underline{\theta} = \theta_{1,1} + \theta_{2,2} = \chi_{1,2} - \chi_{2,1} = -\operatorname{rot} \underline{\chi}, \quad (2.23)$$

$$\|\underline{\theta}\|_{H^1(\Omega)} \leq c \|\operatorname{rot} \underline{\chi}\|_{L^2(\Omega)}. \quad (2.24)$$

By definition of $H_0(\operatorname{rot}; \Omega)$, $\int_{\partial\Omega} \underline{\chi} \cdot \underline{\tau} ds = \int_{\Omega} \operatorname{rot} \underline{\chi} d\Omega = 0 \Rightarrow \int_{\Omega} \nabla \cdot \underline{\theta} d\Omega = 0$, which guarantees that such $\underline{\theta}$ can always be found as a solution to the well-known potential problem (e.g., Ch. 1, Sec. 2.1 of [33]).

4. Set $\underline{\eta} = (-\theta_2, \theta_1)$. Then

$$\operatorname{rot} \underline{\eta} = \theta_{2,2} + \theta_{1,1} = \nabla \cdot \underline{\theta} = -\operatorname{rot} \underline{\chi}, \quad (2.25)$$

and from (2.24), using $\|\operatorname{rot} \underline{\chi}\|_{L^2(\Omega)} \leq \|\underline{\chi}\|_{\Gamma}$, we obtain

$$\|\underline{\eta}\|_{H^1(\Omega)} = \|\underline{\theta}\|_{H^1(\Omega)} \leq c \|\operatorname{rot} \underline{\chi}\|_{L^2(\Omega)} \leq c \|\underline{\chi}\|_{\Gamma} \quad (2.26)$$

5. Take

$$\xi \in H_0^1(\Omega) : \xi = \Delta^{-1} (\nabla \cdot \underline{\chi} + \nabla \cdot \underline{\eta}). \quad (2.27)$$

(Note that both $\nabla \cdot \underline{\chi}$ and $\nabla \cdot \underline{\eta}$ lie in $H^{-1}(\Omega)$). Then

$$\begin{aligned} \|\xi\|_{H^1(\Omega)} &\leq c \|\nabla \cdot \underline{\chi} + \nabla \cdot \underline{\eta}\|_{H^{-1}(\Omega)} \leq c \left(\|\underline{\chi}\|_{L^2(\Omega)} + \|\underline{\eta}\|_{L^2(\Omega)} \right) \leq \\ &\leq c \left(\|\underline{\chi}\|_{L^2(\Omega)} + \|\underline{\eta}\|_{H^1(\Omega)} \right) \stackrel{\text{by (2.26)}}{\leq} c \|\underline{\chi}\|_{\Gamma} \end{aligned} \quad (2.28)$$

6. From (2.27) we have

$$\nabla \cdot \underline{\chi} = \nabla \cdot (\nabla \xi - \underline{\eta}). \quad (2.29)$$

Moreover, using (2.25) in the form⁴

$$\text{rot } \underline{\chi} = \text{rot} (\nabla \xi - \underline{\eta}) \quad (2.30)$$

we obtain a system of PDE's (2.29-2.30) with a boundary condition, given by $\underline{\chi} \cdot \underline{\tau} = 0$ on $\partial\Omega$, which leads to the solution

$$\underline{\chi} = \nabla \xi - \underline{\eta}. \quad (2.31)$$

From equations (2.26) and (2.28)

$$\left(\|\underline{\eta}\|_{H^1(\Omega)} + \|\xi\|_{H^1(\Omega)} \right) \leq c \|\underline{\chi}\|_{\Gamma} \text{ with } c \text{ independent of } \underline{\chi}. \quad (2.32)$$

7. From part 2 we have that

$$\begin{aligned} \|\underline{\gamma}(t)\|_{\Gamma}, \|\underline{\chi}\|_{\Gamma} &= (\underline{\gamma}(t), \underline{\chi}) \stackrel{\text{by (2.31)} \rightarrow (2.19)}{=} (g, \xi) - a(\underline{\beta}, \underline{\eta}) \stackrel{(2.21)}{\leq} \\ &\leq c \left(\|\underline{\eta}\|_{H^1(\Omega)} + \|\xi\|_{H^1(\Omega)} \right) \leq c \|\underline{\chi}\|_{\Gamma}, \end{aligned}$$

⁴Here we invoked the equality $\text{rot } \nabla \varphi = \nabla \times \nabla \varphi = 0$ for any scalar function φ .

which immediately implies (2.20). \square

Remark. In part 6 of the proof, we have shown that for all $\underline{\chi}$ in Γ , it is always possible to find a pair $(\underline{\eta}, \underline{\xi})$ in V , such that (2.31) and (2.32) hold, that is, the map $B_\gamma : V \rightarrow \Gamma$, $B_\gamma \underline{v} = \nabla \underline{\eta} - \underline{\xi} = \underline{\chi} \in \Gamma$ is surjective (we will use this result later). Clearly, the destination space will not change if we multiply the result of the map B_γ by a finite constant, say, $\frac{Gk}{t^2}$, with $t \neq 0$ being a finite number. Now, we have identified that the subspace $\mathcal{G} \subseteq [L^2(\Omega)]^2$, which was used in the formulation (2.17), is, in fact, $H(\text{rot}; \Omega)$. Summarizing, we have proven that in case of finite thickness shears belong to the space $H(\text{rot}; \Omega)$, defined in (2.22), while $H^{-1}(\text{div}; \Omega)$, given by (2.18) becomes appropriate in the limit case $t = 0$. \square

2.4.3 Existence and uniqueness of the solution for FEM with Lagrange multipliers.

The variational form (2.19), in fact, represents a typical case of the well-studied saddle-point optimization problem of the Lagrangian functional:

$$\begin{aligned} (\underline{u}, \underline{\gamma}) &= \inf_{\underline{v}=(\underline{\eta}, \underline{\xi}) \in V} \sup_{\underline{\varsigma} \in \Gamma'} \mathcal{L}(\underline{v}, \underline{\varsigma}), \text{ where} \\ \mathcal{L}(\underline{v}, \underline{\chi}) &= \left\{ \frac{1}{2} a(\underline{v}, \underline{v}) + b(\underline{\varsigma}, \underline{v}) - \langle \underline{g}, \underline{v} \rangle_{V' \times V} - \langle \underline{q}, \underline{\varsigma} \rangle_{\Gamma \times \Gamma'} \right\} \end{aligned} \tag{2.33}$$

(see the original papers [13], [2], and a broad discussion in [18]). In this form $\underline{\varsigma}$ stands for Lagrange multipliers associated with constraint (2.14), which have a physical meaning of shear stresses in the plate.

Remark. The equivalence of the Lagrangian formulation to the problem (2.19) can be shown, if we evoke the necessary conditions for stationarity of

$\mathcal{L}(\underline{v}, \underline{\varsigma})$ at the point $(\underline{u}, \underline{\gamma})$, taking $\underline{q} = \underline{0}$:

$$\begin{cases} a(\underline{u}, \underline{v}) + b(\underline{\gamma}, \underline{v}) - \langle \underline{q}, \underline{v} \rangle_{V' \times V} = 0 & \forall \underline{v} \in V; \\ b(\underline{\varsigma}, \underline{u}) - \langle \underline{q}, \underline{\varsigma} \rangle_{\Gamma \times \Gamma'} = 0 & \forall \underline{\varsigma} \in \Gamma'. \square \end{cases}$$

Here we present a brief discussion on the conditions for existence and uniqueness of the FEM solution in the problems of optimization of a quadratic functional under a linear constraint (2.33) (in our case the functional is given by (2.10), and the corresponding constraint is given by (2.14)).

Example. Saddle-point problem.

In this example we will consider a simpler problem. Assume that we are supposed to find $J^* = \min_{x=\frac{1}{2}} J(x) = \frac{1}{2}x^2$. Trivially, $J^* = J\left(\frac{1}{2}\right) = \frac{1}{8}$. To proceed with Lagrange method, we introduce a Lagrange multiplier y and Lagrangian $L(x, y) = J(x) - y\left(x - \frac{1}{2}\right)$. Invoking stationarity conditions, we have

$$\begin{cases} \frac{\partial L(x, y)}{\partial y} \Big|_{(x^*, y^*)} = x^* - \frac{1}{2} = 0 \Rightarrow x^* = \frac{1}{2}, \\ \frac{\partial L(x, y)}{\partial x} \Big|_{(x^*, y^*)} = x^* - y^* = 0 \Rightarrow y^* = x^* = \frac{1}{2}, \end{cases}$$

and $\min_{x, y} L(x, y) = L\left(\frac{1}{2}, \frac{1}{2}\right) = \frac{1}{8} = J^*$. The functional is shown in the Fig. 2-3. We thus have a saddle point at (x^*, y^*) , such that $L(x, r(x)) \leq L(x^*, y^*) \leq L(x, s(x))$, where $r(x)$ and $s(x)$ are the equations describing the unstable and stable manifold of the saddle surface respectively. This problem is equivalent to $\min_x \left(\sup_y L(x, y) \right)$. To show the equivalence:

$$\sup_y L(x, y) = \begin{cases} \infty, & x \neq \frac{1}{2} \\ J(x), & x = \frac{1}{2} \end{cases}$$

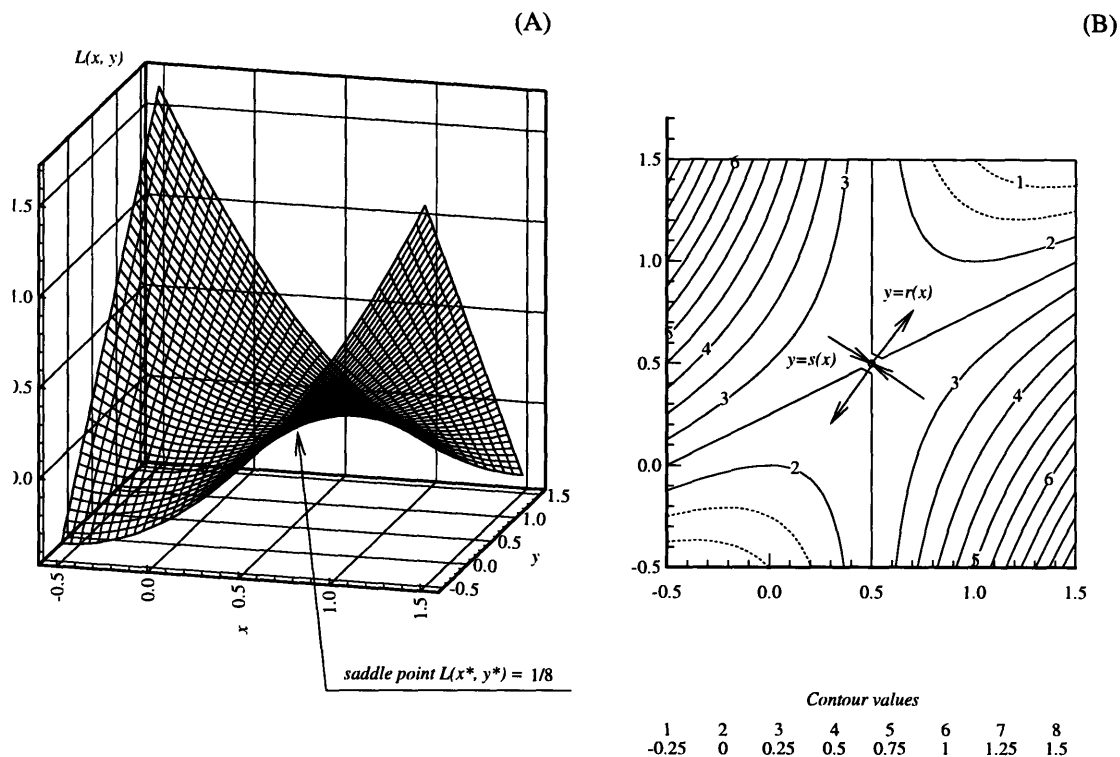


Figure 2-3: (A) - the saddle-point problem; (B) - contour plot of the saddle surface.

$$\min_x \sup_y L(x, y) = \min_x J(x) = \frac{1}{8}. \quad \square$$

The bilinear form $a(\cdot, \cdot)$ defines a symmetric linear operator $A : V \rightarrow V'$, such that $a(\underline{u}, \underline{v}) = \langle A\underline{u}, \underline{v} \rangle_{V' \times V} = \langle \underline{u}, A\underline{v} \rangle_{V \times V'}$. We also introduce a formal operator associated with the bilinear form $b(\cdot, \cdot)$, $B_\gamma : V \rightarrow \Gamma$ and its transpose $B_\gamma^T : \Gamma' \rightarrow V'$

$$\begin{array}{ccc} \Gamma' & \xrightarrow{B_\gamma^T} & V' \\ \updownarrow & & \updownarrow \\ \Gamma & \xleftarrow{B_\gamma} & V \end{array}$$

Then

$$b(\underline{\zeta}, \underline{v}) = (\underline{\zeta}, \nabla \xi - \underline{\eta}) = \langle \underline{\zeta}, B_\gamma (\nabla \xi - \underline{\eta}) \rangle_{\Gamma' \times \Gamma} = \langle B_\gamma^T \underline{\zeta}, \nabla \xi - \underline{\eta} \rangle_{V' \times V},$$

and now we can rewrite the original problem (2.33) in the operator form:

$$\begin{cases} A\underline{u} + B_\gamma^T \underline{\gamma} = \underline{g} \in V', \\ B_\gamma \underline{u} = \underline{q} \in \Gamma. \end{cases}$$

Moreover, let us denote the null space of B_γ as $\text{Ker}(B_\gamma)$, and the range of B_γ as $\mathcal{R}(B_\gamma)$. Then we have the following very intuitive result that follows directly from the Lax-Milgram theorem [22].

Proposition 1. Let $\underline{q} \in \mathcal{R}(B_\gamma)$ and the bilinear form $a(\cdot, \cdot)$ be elliptic on $\text{Ker}(B_\gamma)$, namely

$$\exists \alpha_0 > 0 \text{ such that } a(\underline{v}, \underline{v}) \geq \alpha_0 \|\underline{v}\|_V \quad \forall \underline{v} \in \text{Ker}(B_\gamma). \quad (2.34)$$

Then there exists a unique $\underline{u} \in V$, such that

$$\begin{cases} a(\underline{u}, \underline{v}) = \langle \underline{g}, \underline{v} \rangle_{V' \times V} \quad \forall \underline{v} \in \text{Ker}(B_\gamma), \text{ and} \\ b(\underline{\zeta}, \underline{u}) = \langle \underline{\zeta}, \underline{q} \rangle_{\Gamma' \times \Gamma} \quad \forall \underline{\zeta} \in \Gamma'. \end{cases} \quad (2.35)$$

For the proof we refer to [18].

Proposition 1 implies that if the first component of solution, \underline{u} , exists, it is unique. Condition (2.34) states the restrictions that we have to impose on the reduction operator R_h in (2.15) to obtain a unique \underline{u} (a number of reduced-integrated elements violating this condition were proposed in earlier publications on the subject, see e.g., [29]).

Now we turn to the problem of finding the Lagrange multipliers, $\underline{\gamma}$. For this we have to make the following restrictions on B_γ , namely, we require $\mathcal{R}(B_\gamma)$ to

be closed in Γ .

Remark. Closed range operators. The concept of a closed range operator is a generalization of the idea of a bounded linear function. Moreover, *the Closed Graph Theorem* states that if the range of an operator $\mathcal{R}(f)$, $f : A \rightarrow B$, where A and B are some Sobolev spaces, is closed in B , then f is continuous on its domain $\mathcal{D}(f) = A$. \square

Now we can apply results of Banach's closed range theorem:

Proposition 2. The following statements are equivalent:

- (i) $\mathcal{R}(B_\gamma)$ is closed in Γ ;
- (ii) $\mathcal{R}(B_\gamma^T)$ is closed in V' ;
- (iii) $\exists k_0 > 0$ such that $\forall \underline{q} \in \mathcal{R}(B_\gamma)$, $\exists v_q \in V$:

$$B_\gamma v_q = \underline{q}, \quad \|v_q\|_V \leq \frac{1}{k_0} \|\underline{q}\|_\Gamma;$$

- (iv) $\exists k_0 > 0$ such that $\forall \underline{g} \in \mathcal{R}(B_\gamma^T)$, $\exists \underline{\gamma}_f \in \Gamma'$:

$$B_\gamma^T \underline{\gamma}_f = \underline{g}, \quad \|\underline{\gamma}_f\|_{\Gamma'} \leq \frac{1}{k_0} \|\underline{g}\|_{V'}.$$

For the proof of (i)-(iv) we refer to [5].

Remark. Basically, the closed range theorem is the straightforward extension of the closed graph theorem mentioned above. The most valuable addition to the continuity of B_γ (which is implied by (i) according to the closed graph theorem, and equivalent to saying (iii)), is the dual result for B_γ^T . \square

Now we can clearly define the norm over V' using duality arguments:

$$\|\underline{g}\|_{V'} = \sup_{\underline{v} \in V, \underline{v} \neq 0} \frac{|\langle \underline{g}, \underline{v} \rangle_{V' \times V}|}{\|\underline{v}\|_V};$$

and substituting this into equation (iv), we obtain the inf-sup condition as follows:

$$\begin{aligned} \|\underline{g}\|_{V'} &= \sup_{\underline{v} \in V, \underline{v} \neq \underline{0}} \frac{|\langle \underline{g}, \underline{v} \rangle_{V' \times V}|}{\|\underline{v}\|_V} = \sup_{\underline{v} \in V, \underline{v} \neq \underline{0}} \frac{|\langle B_\gamma^T \underline{\gamma}, \underline{v} \rangle_{V' \times V}|}{\|\underline{v}\|_V} = \\ &= \sup_{\underline{v} \in V, \underline{v} \neq \underline{0}} \frac{b(\underline{\gamma}, \underline{v})}{\|\underline{v}\|_V} \geq k_0 \|\underline{\gamma}\|_{\Gamma'}, \quad \forall \underline{\gamma} \in \Gamma', \underline{\gamma} \neq \underline{0}. \end{aligned} \quad (2.36)$$

Now we can summarize the results of propositions 1 and 2.

Proposition 3. Let the continuous bilinear form $a(\cdot, \cdot)$ be elliptic on $\text{Ker}(B_\gamma)$ (that is, (2.34) holds). Moreover, let us suppose that the range of the formal operator associated with the bilinear form $b(\cdot, \cdot)$ is closed in Γ . Then there exists a solution to the problem of type (2.33) for any $\underline{g} \in V'$ and $\underline{q} \in \mathcal{R}(B_\gamma)$.

Proof. Let $\underline{q} \in \mathcal{R}(B_\gamma)$ and \underline{u} be the unique solution of the auxiliary problem (2.35). We need to show that if $\mathcal{R}(B_\gamma)$ is closed in Γ , then for all $\underline{g} \in \mathcal{R}(B_\gamma^T)$ there exists $\underline{\gamma} \in \Gamma'$, such that $(\underline{u}, \underline{\gamma})$ is the solution for (2.33).

Consider the linear functional on $V : L(\underline{v}) \in \mathcal{R}(B_\gamma^T) \subset V' :$

$$L(\underline{v}) = -a(\underline{u}, \underline{v}) + \langle \underline{g}, \underline{v} \rangle_{V' \times V}.$$

Firstly, take $\underline{v}_0 \in \text{Ker}(B_\gamma)$; clearly, by (2.35), $L(\underline{v}_0) = 0 \forall \underline{v}_0 \in \text{Ker}(B_\gamma)$, so we indeed have a solution for that case.

Next, if $\underline{v} \notin \text{Ker}(B_\gamma)$ then by (ii) in Proposition 2, the $\mathcal{R}(B_\gamma^T)$ is closed in V' ; this implies (by (iv) in Proposition 2) that there exists $\underline{\gamma} \in \Gamma'$, such that $L(\underline{v}) = b(\underline{\gamma}, \underline{v})$. \square

Remark. It could be shown that the inf-sup condition (2.36) along with the ellipticity condition (2.34) represent sufficient and necessary conditions not only for existence and uniqueness but also for *optimality* of the solution for the saddle-problem optimization (2.33) (see e.g. Theorem 1.1 in [18] and a broad discussion in [14]). The deeper insight into the physical meaning of the inf-sup condition can be found in [6]. \square

Chapter 3

MITC plate bending elements.

3.1 Design principles.

In this section we present the design principles for the MITC family of plate bending elements, based on the RM-model and mixed interpolation. These results are adopted from original papers [15], [8].

3.1.1 Preliminary considerations.

For the further analysis we shall consider the limit, and therefore, most severe case $t = 0$, presuming, that if our finite element discretization provides a good solution for that case, then the elements will not lock in any other case.

Summarizing the results of the previous chapter, in the limit $t = 0$ we face the following *modified discrete variational problem*:

$$\begin{aligned} & \text{Find } \underline{u}_h = (\underline{\beta}_h, w_h) \in V_h = B_h \times W_h \text{ and } \underline{\gamma}_h \in \mathcal{G}_h = R_h(B_h \cup \nabla W_h), \text{ such that} \\ & \left\{ \begin{array}{l} a(\underline{\beta}_h, \underline{\eta}_h) + (\underline{\gamma}_h, R_h(\nabla \xi_h - \underline{\eta}_h)) = (g, \xi_h) \quad \forall \underline{v}_h = (\underline{\eta}_h, \xi_h) \in V_h, \\ (\underline{\chi}_h, R_h(\nabla \xi_h - \underline{\eta}_h)) = 0 \quad \forall \underline{\chi}_h \in \mathcal{G}_h. \end{array} \right. \end{aligned} \tag{3.1}$$

Moreover, as we have shown in section 2.4.3, we obtain a unique solution for \underline{u}_h , if

$$\exists \alpha_0 > 0 : a(\underline{\eta}_h, \underline{\eta}_h) \geq \alpha_0 \|\underline{v}_h\|_V \quad \forall \underline{v}_h = (\underline{\eta}_h, \xi_h) \in \text{Ker}(R_h B_\gamma), \quad (3.2)$$

and a unique and stable solution for $\underline{\gamma}_h$ if

$$\exists k_0 > 0 : \inf_{\underline{\chi}_h \in \mathcal{G}_h, \underline{\chi}_h \neq \underline{0}} \sup_{\underline{v}_h \in V_h, \underline{v}_h \neq \underline{0}} \frac{(\underline{\chi}_h, R_h(\nabla \xi_h - \underline{\eta}_h))}{\|\underline{\chi}_h\|_{\Gamma'} \|\underline{v}_h\|_V} \geq k_0, \quad (3.3)$$

where

$$\|\underline{\chi}_h\|_{\Gamma'} = \sup_{\underline{\gamma} \in \Gamma, \underline{\gamma} \neq \underline{0}} \frac{\langle \underline{\chi}_h, \underline{\gamma} \rangle_{\Gamma' \times \Gamma}}{\|\underline{\gamma}\|_{\Gamma}} = \sup_{\underline{\gamma} \in \Gamma, \underline{\gamma} \neq \underline{0}} \frac{(\underline{\chi}_h, \underline{\gamma})}{\|\underline{\gamma}\|_{\Gamma}}.$$

Clearly, the choice of the functional spaces V_h , \mathcal{G}_h , and the reduction operator R_h is of great importance, and determines existence and behavior of the solution.

Let us make the first step that puts some structure on R_h and is crucial for the formulation of the elements. We choose $R_h : V_h \rightarrow \mathcal{G}_h$ to satisfy

$$(R_h - I) \nabla \xi_h = \underline{0} \quad \forall \xi_h \in W_h, \quad (3.4)$$

$$\exists c \geq 0 : \|R_h \underline{\eta}_h\|_{H^1(\Omega)} \leq c \|\underline{\eta}_h\|_{H^1(\Omega)}, \quad (3.5)$$

where $\mathcal{G}_h \equiv \Gamma_h$ is a subspace of the functional space Γ introduced in Section 2.4.2.

Remark. Condition (3.5) just enforces the continuity of the operator, and is quite natural due to the physics of the problem, while (3.4) is a rather strict condition which implies that we shall use the standard interpolation for the gradient of the transverse displacement field. This condition is sufficient, but not necessary to allow us to use the "energy-type" seminorm, defined on V by

$$|\underline{v}|_V^2 = \mathcal{A}(\underline{v}, \underline{v}) \geq |\underline{\eta}|_{H^1(\Omega)}^2 + \|R_h(\nabla \xi_h - \underline{\eta}_h)\|_{L^2(\Omega)}^2, \quad (3.6)$$

as a norm, and thus, to be sure that the property (3.2) holds. Another possible condition would be, for instance (see [41]),

$$R_h \nabla \xi_h = \underline{0} \Rightarrow \xi_h = 0 \quad \forall \xi_h \in W_h. \quad \square$$

In the limit case our approximate solution should satisfy the Kirchhoff constraint (2.14), that is

$$R_h (\underline{\eta}_h - \nabla \xi_h) = 0 \Leftrightarrow R_h \underline{\eta}_h = R_h \nabla \xi_h \stackrel{\text{by (3.5)}}{=} \nabla \xi_h. \quad (3.7)$$

Noting that

$$\text{rot } \nabla \xi_h = \text{rot} \left(\frac{\partial \xi_h}{\partial x_1}, \frac{\partial \xi_h}{\partial x_2} \right) = -\frac{\partial^2 \xi_h}{\partial x_2 \partial x_1} + \frac{\partial^2 \xi_h}{\partial x_1 \partial x_2} = 0 \quad \forall \xi_h \in W_h, \quad (3.8)$$

we obtain

$$\text{rot } \nabla \xi_h = 0 \stackrel{\text{by (3.7)}}{\Rightarrow} \text{rot } R_h \underline{\eta}_h = 0. \quad (3.9)$$

3.1.2 Stokes analogy.

For the time being, we consider a slightly different constraint, namely,

$$\left\{ (q, \text{rot } \underline{\eta}_h) = 0 \quad \forall q \in Q_h \subset Q = L^2(\Omega) \right\} \Leftrightarrow P_h \text{rot } \underline{\eta}_h = 0, \quad (3.10)$$

where $P_h(\cdot)$ stands for the L^2 -projection, and Q is an auxiliary space.

Note that the rot-operator introduced in (2.22) is close to the divergence operator, namely, for any scalar function a and vector function \underline{v} :

$$\begin{aligned} (\text{rot } a)^\perp &= \nabla a, & \text{rot } (\underline{v}^\perp) &= -\nabla \cdot \underline{v}, \\ \text{rot } a &= -(\nabla a)^\perp, & \text{rot } \underline{v} &= \nabla \cdot (\underline{v}^\perp), \end{aligned} \quad (3.11)$$

where " \perp " stands for the ninety degree clockwise rotation of the vector argument.

Thus, we are clearly facing a minimization problem under the constraint similar to the one encountered in the analysis of an incompressible flow.

The results for the well-studied Stokes problem (see, e.g. [18]) will serve us as a starting point in the further elements' construction. The mixed discrete variational problem corresponding to the Stokes flow with homogeneous boundary conditions is:

Find $\underline{u}_h \in V_h^S \subset V^S = [H_0^1(\Omega)]$, $p_h \in Q_h^S \subset Q^S = L^2(\Omega)$, such that

$$\begin{cases} a^S(\underline{u}_h, \underline{v}_h) + b^S(\underline{v}_h, p_h) = (\underline{f}_h, \underline{v}_h), & \forall \underline{v}_h \in V_h^S, \\ b^S(\underline{u}_h, q_h) = 0, & \forall q_h \in Q_h^S, \end{cases} \quad (3.12)$$

where $a^S(\underline{u}, \underline{v}) = 2\mu \int_{\Omega} \underline{\varepsilon}(\underline{u}) \cdot \underline{\varepsilon}(\underline{v}) d\Omega$, and $b^S(\underline{v}, q) = - \int_{\Omega} q(\nabla \cdot \underline{v}) d\Omega$ (super-script "S" stands for "Stokes" in further considerations). Let us note that the bilinear form $a^S(\cdot, \cdot)$ is always elliptic, so that we do not need to worry about existence and uniqueness of the solution for the velocity field \underline{u}_h .

To have a unique solution for pressure distribution p_h , the discrete spaces V_h^S and Q_h^S should satisfy the stability inequality

$$\sup_{\underline{v}_h \in V_h^S, \underline{v}_h \neq \underline{0}} \frac{b^S(\underline{v}_h, q_h)}{\|\underline{v}_h\|_{V^S}} \geq c(h, k) \|q_h\|_{Q^S}, \quad \forall q_h \neq 0 \in Q_h^S, \quad (3.13)$$

with a positive constant $c(h, k)$ depending as little as possible on the mesh size h and degree of polynomials k used as Galerkin basis functions (satisfaction of this inequality guarantees that the range of operator, associated with $b^S(\cdot, \cdot)$ is closed in Q' for some fixed values of h and k). Note that if this constant is independent of the mesh size h , then we have the inf-sup condition of the form

$$\inf_{q_h \in Q_h^S, q_h \neq 0} \sup_{\underline{v}_h \in V_h^S, \underline{v}_h \neq \underline{0}} \frac{b^S(\underline{v}_h, q_h)}{\|q_h\|_{Q^S} \|\underline{v}_h\|_{V^S}} \geq k_0, \quad (3.14)$$

and our solution for \underline{u}_h and p_h in (3.12) is stable and optimally convergent in the corresponding norms. There exist quite a few such pairs (V_h^S, Q_h^S) described in the literature, that are known to satisfy the inf-sup condition (3.14) (e.g., RT-spaces [42], BDM-spaces [16], BDFM-spaces [17]).

To see the analogy between the original problem and the Stokes problem, we take $\underline{u}_h = \underline{\beta}_h^\perp \in B_h^\perp$. Then, we have

$$\begin{aligned} b^S(\underline{u}_h, q_h) &= -\left(q_h, \nabla \cdot (\underline{\beta}_h^\perp)\right) \stackrel{\text{use (3.11)}}{=} -\left(q_h, \text{rot } \underline{\beta}_h\right) = 0 \quad \forall q_h \in Q_h^S \Leftrightarrow \\ &\Leftrightarrow P_h \text{rot } \underline{\beta}_h = 0, \end{aligned}$$

which is nothing else, but the constraint (3.10). Noticing firstly that rotation is an affine transformation, which preserves all properties of a space under consideration, and secondly, that the stability condition (3.13) does not depend on the bilinear form $a^S(\cdot, \cdot)$, we conclude that to have a unique and stable solution of the Stokes-like problem

$$\begin{cases} a(\underline{\beta}_h, \underline{\eta}_h) - (p_h, \text{rot } \underline{\eta}_h) = 0 & \forall \underline{\eta}_h \in B_h, \\ (q_h, \text{rot } (\underline{\beta}_h - \underline{\gamma}_h)) = 0 & \forall \underline{q}_h \in Q_h \end{cases} \quad (3.15)$$

for the pair $(\underline{\beta}_h, p_h)$, we should satisfy the stability condition

$$\sup_{\underline{\eta}_h \in B_h, \underline{\eta}_h \neq 0} \frac{(q_h, \text{rot } \underline{\eta}_h)}{\|\underline{\eta}_h\|_V} \geq c(h, k) \|q_h\|_Q, \quad \forall q_h \neq 0 \in Q_h,$$

and the corresponding inf-sup condition for the optimal convergence

$$\inf_{q_h \in Q_h, q_h \neq 0} \sup_{\underline{\eta}_h \in B_h, \underline{\eta}_h \neq 0} \frac{(q_h, \text{rot } \underline{\eta}_h)}{\|q_h\|_Q \|\underline{\eta}_h\|_V} \geq k_0.$$

3.1.3 Construction of the elements.

Clearly, using a pair (B_h, Q_h) , that is known to work for the rotated Stokes problem (and correspondingly, for the problem (3.15)), namely, satisfying the inf-sup condition (3.14), or, at least the stability condition (3.13) with $\underline{v}_h = \underline{\beta}_h^\perp$, we shall get the space B_h , which will not lock under the constraint (3.10)). The only thing, that we have to do now, is to match our actual constraint (3.9) with the one introduced in (3.10). Recalling that $R_h : B_h \rightarrow \Gamma_h$, we are able now to make the following proposition:

Proposition 3. In case $t = 0$, the following statements are equivalent:

- (i) $\text{rot } R_h \underline{\eta}_h = 0 \quad \forall \underline{\eta}_h \in B_h$; and
- (ii) Commuting diagram property is satisfied, that is:

$$\begin{array}{ccc}
 B_h & \xrightarrow{\text{rot}} & L^2 \\
 R_h \downarrow & & \downarrow P_h \\
 \Gamma_h & \xrightarrow{\text{rot}} & Q_h
 \end{array} \tag{3.16}$$

The proof (i) \Leftrightarrow (ii) is trivial; clearly the commuting diagram states that

$$\text{rot } R_h \underline{\eta}_h = P_h \text{rot } \underline{\eta}_h \stackrel{\text{by (3.10) for } t=0}{=} 0 \quad \forall \underline{\eta}_h \in B_h. \tag{3.17}$$

The commuting diagram (3.16) can also be written as an integral equation (for the limit case):

$$\begin{aligned}
 \text{rot } R_h \underline{\eta}_h = 0 &\Rightarrow (\text{rot } R_h \underline{\eta}_h, q_h) = 0 \quad \forall q_h \in Q_h \Leftrightarrow \\
 &\Leftrightarrow (\text{rot } R_h \underline{\eta}_h, q_h) - P_h \text{rot } \underline{\eta}_h = 0 \Leftrightarrow \\
 &(\text{rot } (R_h \underline{\eta}_h - \underline{\eta}_h), q_h) = 0.
 \end{aligned} \tag{3.18}$$

Noting that conditions (3.4) and (3.8) impose explicit restrictions on the structure of the interpolation space W_h , we are ready to close the loop. Thus, we have the following "algorithm" for the construction of an element:

1. Start with the pair of interpolation spaces (B_h^\perp, Q_h) , that is "good" for the Stokes problem. B_h would be the space for rotations, while Q_h is an auxiliary space, which never appears in actual calculations (by "good" we mean that we satisfy either (3.13) or (3.14)).
2. Find another space Γ_h and an operator R_h , such that the diagram (3.16) commutes.
3. Choose the space for transverse displacements W_h to satisfy (3.4), i.e.

$$\nabla W_h \subset \Gamma_h, \text{rot } \nabla \xi_h = 0 \quad \forall \xi_h \in W_h.$$

Remark 1. Although following the algorithm stated above does not imply that the result of our choice for discrete spaces and reduction operator would satisfy the inf-sup condition (3.3), the elliptic properties of the form $\mathcal{A}(\cdot, \cdot)$ are clearly preserved by imposition of (3.4). \square

Remark 2. Stability condition vs. the Inf-sup condition. As we pointed above, the space Q_h does not have any physical meaning, and serves just as a link between the Stokes problem and the problem of interest. The stability condition (3.13) ensures that the solution for $\underline{\beta}_h$ will be stable and accurate, while condition (3.14) guarantees that *both* $\underline{\beta}_h$ and p_h are optimally convergent. Certainly, we are barely interested in p_h 's, therefore (3.14) is in fact too strong, and we should not discard pairs (B_h^\perp, Q_h) that are known to work for velocities but fail for pressures in the analysis of the Stokes flow (as an example of such a pair we can take the $Q_1 - P_0$ pair, which serves as a basis for the MITC4 element construction). \square

3.1.4 Justification.

A reasonable question that one can ask now is – why do we need to follow such a long way if we do not gain anything (i.e., the inf-sup condition may not be satisfied, etc.)?

The following result ([18]), though, states that we have obtained at least some optimality.

Proposition 4. The operator R_h defined in (3.4) and (3.5) is surjective on Γ_h .

Proof. All we need to prove is that for every $\underline{\gamma}_h \in \Gamma_h$, we can find a pair $(\underline{\beta}_h, w_h) \in B_h \times W_h = V_h$, such that

$$\begin{aligned} R_h(\nabla w_h - \underline{\beta}_h) &= \underline{\gamma}_h, \\ \|w_h\|_{H^1} + \|\underline{\beta}_h\|_{H^1} &\leq c \|\underline{\gamma}_h\|_{\Gamma_h}. \end{aligned}$$

To show this, we shall follow the algorithm described above. Firstly, for a given $\underline{\gamma}_h \in \Gamma_h$, we solve the Stokes-like system (3.15) for $\underline{\beta}_h \in B_h$ and an auxiliary variable $p_h \in Q_h$. The fact that we have chosen the pair $B_h \times Q_h$ to satisfy either (3.14) or (3.13) guarantees that there exists a unique $\underline{\beta}_h$, such that $\text{rot } R_h \underline{\beta}_h = \text{rot } \underline{\gamma}_h$, and $\|\underline{\beta}_h\|_{H^1} \leq c \|\underline{\gamma}_h\|_{\Gamma_h}$. If we satisfy the inf-sup condition (3.14), then the constant c is independent of the plate thickness, which is not the case if only (3.13) holds. Having that $\text{rot}(\underline{\gamma}_h - R_h \underline{\beta}_h) = 0$, we can find $w_h \in W_h$, such that $\nabla w_h = \underline{\gamma}_h - R_h \underline{\beta}_h$.

For example, the appropriate w_h can be uniquely determined as the solution of the discrete variational problem $(\nabla w_h, \nabla \psi_h) = (\underline{\gamma}_h - R_h \underline{\beta}_h, \nabla \psi_h) \quad \forall \psi_h \in W_h$. Continuity of R_h stated in (3.4) ensures that $\|w_h\|_{H^1} \leq c \|\underline{\gamma}_h\|_{\Gamma_h}$, therefore allowing us to conclude the proof. \square

Remark 1. Surjective maps. Inf-sup condition in the Γ'_h norm. A function $f : A \rightarrow B$ is *surjective* if and only if every b in B is the image of some

element of A (a geometrical interpretation is shown on Fig. 3-1). It can be shown

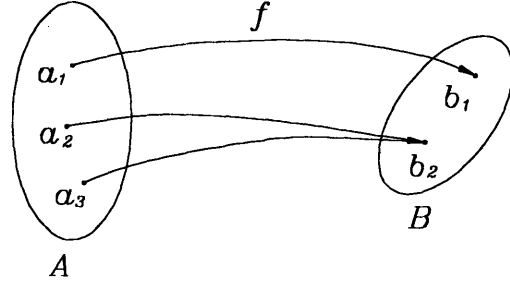


Figure 3-1: Surjective function.

(see any elementary course on functional analysis, e.g. [38]), that surjectivity of the function f is sufficient to guarantee that its range $\mathcal{R}(f)$ is closed in B . Therefore, Proposition 4 implicitly states that the range of R_h is closed in Γ_h , and we have that

$$\exists k > 0 : \sup_{\underline{v}_h \in V_h, \underline{v}_h \neq 0} \frac{(\underline{x}_h, R_h(\nabla \xi_h - \eta_h))}{\|\underline{v}_h\|_V} \geq k \|\underline{x}_h\|_{\Gamma_h} \quad \forall \underline{x}_h \in \Gamma_h, \quad (3.19)$$

where

$$\|\underline{x}_h\|_{\Gamma_h} = \sup_{\underline{\gamma}_h \in \Gamma_h, \underline{\gamma}_h \neq 0} \frac{(\underline{\gamma}_h, \underline{x}_h)}{\|\underline{\gamma}_h\|_{\Gamma_h}}. \quad (3.20)$$

If the constant k , appearing on the r.h.s. of (3.19), does not depend on the thickness t , then we obtain nothing else but a discrete form of the inf-sup condition (3.3), or *the inf-sup condition in the Γ_h -norm*. Although this result is weaker than the original condition, in practical calculations we deal with finite-dimensional operators rather than with infinite-dimensional maps, and therefore, by now, we have obtained quite satisfactory optimality. Moreover, it can be shown that the elements, designed using the algorithm stated above, are optimally convergent in the sense of the norm (3.20), see [18]. Let us finally note that k will be clearly independent on t if the starting pair of spaces (B_h, Q_h) satisfies the inf-sup con-

dition for the rotated Stokes problem (it might not be the case if we satisfy only (3.13)). \square

Remark 2: Discrete vs. continuous inf-sup condition.

If our elements satisfy the discrete inf-sup condition (3.19) in the Γ'_h -norm, then the sufficient condition to satisfy it in the continuous form (3.3), is :

$$\|\underline{\gamma}_h\|_{\Gamma'_h} = \rho \|\underline{\gamma}_h\|_{\Gamma'}, \quad \forall \underline{\gamma}_h \in \Gamma'_h, \quad (3.21)$$

with ρ being a constant independent of the mesh size and plate thickness. \square

3.2 The elements.

In this section we describe the standard approach to the plate bending problem, as well as the MITC family of plate bending elements, taking the MITC4 and MITC9 elements as typical representatives.

3.2.1 Reference element and covariant transformation.

In the following analysis all discrete finite element spaces are defined from the corresponding spaces on the reference square element $\widehat{K} = (-1, 1)^2$ through a covariant tensor transformation. The reduction operator is R_h^K also defined locally on each element K , which allows us to construct it for general elements using a covariant transformation of the operator \widehat{R}_h defined over \widehat{K} . This enables us, without loss of generality, to consider all operations only over \widehat{K} , then extending the results to more general cases. Let J^K be the Jacobian matrix, associated with the transformation of the K -th element; its determinant is $\Delta^K = \det(J^K)$ (Fig. 3-2).

A fairly standard assumption on J^K is the existence of its inverse $(J^K)^{-1}$ for

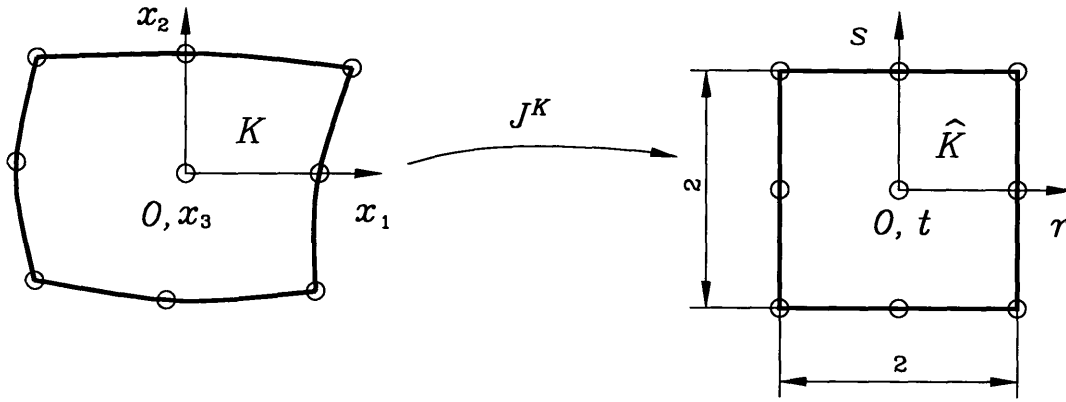


Figure 3-2: Covariant transformation of a general element.

each $K = 1..N$. Moreover, as the characteristic mesh size $h \rightarrow 0$, we have

$$\max_K \left\| \left(J^K \right)_{ij}^{-1} \right\|_{L^\infty(K)} \leq C < \infty, \quad i, j = 1..2, K = 1..N.$$

These assumptions ensure that all maps are well-defined in the sense that we cannot have singularities of the FEM matrices due to the use of general elements.

3.2.2 Displacement-based finite elements.

The simplicity of these elements made them popular in the finite element analysis of plates, although the results are often far from reality, because of locking. The space for shears is obtained as (taking the reduction operator as an identity transformation)

$$\mathcal{G}_h = \Gamma_h = \nabla W_h \cup B_h,$$

which implies that

$$\text{Ker}(R_h B_\gamma) = \text{Ker}(B_\gamma) = \left\{ \underline{v}_h = (\underline{\eta}_h, \xi_h) \in V_h \mid \nabla \xi_h = \underline{\eta}_h \right\}.$$

This condition severely restricts the space of interpolation functions, which satisfy the discrete Kirchhoff constraint (the worst results are obtained for lower order elements, namely $P3$ and $Q4$ elements; see Appendix A for numerical examples), barely leaving a hope to obtain uniformly good convergence for all thicknesses t . We omit the details of construction of the FEM matrices, though referring to Sec. 5.4 of [6].

3.2.3 MITC4 element.

The element was initially presented in [24] as a shell element. Numerical performance, mathematical analysis, error estimates, and convergence rates are shown in the subsequent publications, e.g., [10], [7].

For the mixed-interpolated 4-node element we use (taking homogeneous boundary conditions for the sake of simplicity):

$$\begin{aligned}
W_h &= \left\{ \xi_h : \xi_h \in H_0^1(\Omega), \xi_h|_{\widehat{K}} \in Q_1(\widehat{K}) \right\}, \\
B_h &= \left\{ \underline{\eta}_h : \underline{\eta}_h \in [H_0^1(\Omega)]^2, \underline{\eta}_h|_{\widehat{K}} \in [Q_1(\widehat{K})]^2 \right\}, \\
Q_h &= \left\{ p_h : p_h|_{\widehat{K}} = \text{const} \right\}, \\
\Gamma_h &= \left\{ \underline{\gamma}_h : \underline{\gamma}_h \in H_0(\text{rot}; \Omega), \underline{\gamma}_h|_{\widehat{K}} \in RT(\widehat{K}) \right\}, \\
RT(\widehat{K}) &= (\text{span}\{1, s\}, \text{span}\{1, r\}).
\end{aligned}$$

The pair (B_h, Q_h) satisfies the stability inequality (3.13) with constant $c(h, k) =$

$O(h)$ (see the proof in [32]). The fact that $p_h|_{\hat{K}} = \text{const}$ implies that

$$\begin{aligned}
& \left(\text{rot} \left(R_h \underline{\eta}_h - \underline{\eta}_h \right), q_h \right) = 0 \quad \forall q_h \in Q_h \Rightarrow \\
& \Rightarrow \int_{\Omega} \text{rot} \left(R_h \underline{\eta}_h - \underline{\eta}_h \right) d\Omega = \int_{\partial\Omega} \left(R_h \underline{\eta}_h - \underline{\eta}_h \right) \cdot \underline{t} dS = \\
& = \sum_{K=1}^N \int_{\partial\hat{K}} \left(\hat{R}_h \underline{\eta}_h - \underline{\eta}_h \right) |_{\hat{K}} \cdot \underline{t} \Delta^K dS|_{\hat{K}} = 0,
\end{aligned} \tag{3.22}$$

where \underline{t} stands for a unit tangential vector.

Using integration along the edges e_i , $i = 1..4$, of the reference element, i.e.,

$$\int_{\partial\hat{K}} f(S) dS|_{\hat{K}} = \sum_{i=1}^4 \int_{e_i} f(l) |_{e_i} dl_i,$$

and using $\Delta^K = \text{const}$ (affine covariant transformations), we can try find the reduction operator \hat{R}_h . The fact that $\underline{\eta}_h|_{\hat{K}}$ is a bilinear vector function allows us to calculate the integral along an edge e_i as

$$\int_{e_i} \left(\hat{R}_h \underline{\eta}_h - \underline{\eta}_h \right) |_{e_i} \cdot \underline{t} dl_i = \int_{e_i} dl_i \left(\hat{R}_h \underline{\eta}_h - \underline{\eta}_h \right) |_{e_i, l_i=0} \cdot \underline{t}.$$

Thus, to obtain zero on the r.h.s. of (3.22), we should construct \hat{R}_h to satisfy $\hat{R}_h \underline{\eta}_h = \underline{\eta}_h$ at the midpoints of every edge e_i (so-called tying procedure). Equivalently,

$$\begin{aligned}
& \nabla \xi_h - \hat{R}_h \underline{\eta}_h = \nabla \xi_h - \underline{\eta}_h \quad \forall \xi_h \in W_h \Leftrightarrow \\
& \Leftrightarrow \hat{R}_h \left(\nabla \xi_h - \underline{\eta}_h \right) = \underline{\gamma}_h = \underline{\gamma}_h^{ST}
\end{aligned}$$

at the edges' midpoints, where $\underline{\gamma}_h \in \Gamma_h$, and $\underline{\gamma}_h^{ST}$ are the values of the shear strains obtained from the standard displacement-based interpolation.

Therefore, by tying shears with displacement-based values at the mid-points of the corresponding edges, we enforce the commuting diagram property to hold.

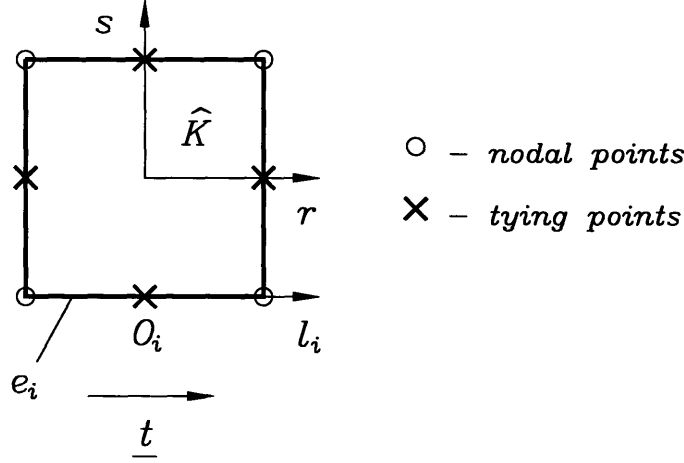


Figure 3-3: Tying procedure for the MITC4 element.

The choice of W_h provides the same order of accuracy as for rotations; moreover we have

$$\nabla W_h = \{ \underline{\sigma}_h : \underline{\sigma}_h|_{\widehat{K}} \subset \Gamma_h, \text{rot } \underline{\sigma}_h = 0 \}.$$

As a result, we obtained a very robust, simple, low-order element, which does not lock for small thicknesses (see Appendix A for numerical results).

3.2.4 MITC9 element.

For the mixed-interpolated nine-node element ([15]), we take

$$\begin{aligned}
 W_h &= \{ \xi_h : \xi_h \in H_0^1(\Omega), \xi_h|_{\widehat{K}} \in Q_2'(\widehat{K}) \}, \\
 B_h &= \{ \underline{\eta}_h : \underline{\eta}_h \in [H_0^1(\Omega)]^2, \underline{\eta}_h|_{\widehat{K}} \in [Q_2(\widehat{K})]^2 \}, \\
 Q_h &= \{ p_h : p_h|_{\widehat{K}} \in P_1(\widehat{K}) \}, \\
 \Gamma_h &= \{ \underline{\gamma}_h : \underline{\gamma}_h \in H_0(\text{rot}; \Omega), \underline{\gamma}_h|_{\widehat{K}} \in BDFM(\widehat{K}) \}, \\
 BDFM(\widehat{K}) &= (\text{span} \{1, r, s, rs, s^2\}, \text{span} \{1, r, s, rs, r^2\}),
 \end{aligned} \tag{3.23}$$

and $Q'_2(\widehat{K})$ is the 2nd order Serendipity space defined over \widehat{K} .

The pair (B_h, Q_h) is known to satisfy the inf-sup condition (3.14). To satisfy the commuting diagram, we have to impose the following restrictions on \widehat{R}_h :

$$\int_{\widehat{K}} (\widehat{R}_h \underline{\eta}_h - \underline{\eta}_h) \Delta^K dr ds = \underline{0}; \text{ and} \quad (3.24)$$

$$\int_{e_i} (\widehat{R}_h \underline{\eta}_h - \underline{\eta}_h) \cdot \underline{t} p(l) \Delta^K dl_i = 0 \quad \forall p(l) \in P_1(\widehat{K})|_{l_i}, e_i, i = 1..4. \quad (3.25)$$

Then

$$\begin{aligned} & \int_{\widehat{K}} \text{rot}(\widehat{R}_h \underline{\eta}_h) q_h dr ds = - \int_{\widehat{K}} (\widehat{R}_h \underline{\eta}_h) \cdot \text{rot} q_h dr ds + \\ & + \int_{\partial \widehat{K}} (\widehat{R}_h \underline{\eta}_h) \cdot \underline{t} q_h dS \stackrel{\text{use (3.23), (3.25)}}{=} \\ & = - \int_{\widehat{K}} (\widehat{R}_h \underline{\eta}_h) \cdot \underbrace{\text{rot} q_h}_{\in \mathbb{R}^2} dr ds + \int_{\partial \widehat{K}} \underline{\eta}_h \cdot \underline{t} q_h dS \stackrel{\text{use (3.24)}}{=} \\ & = - \int_{\widehat{K}} \underline{\eta}_h \cdot \text{rot} q_h dr ds + \int_{\partial \widehat{K}} \underline{\eta}_h \cdot \underline{t} q_h dS = \int_{\widehat{K}} \text{rot}(\underline{\eta}_h) q_h dr ds, \end{aligned}$$

which proves the sufficiency of (3.24) and (3.25). Again, the space W_h has the same order of accuracy as the one for rotations, and $\nabla W_h \subset B_h$.

As we have done for MITC4 element, for $\Delta^K = \text{const}$, we can calculate integrals (3.25) using numerical quadratures (2-point Gauss rule is the best choice).

The MITC9 element is more expensive than the 9-node displacement based element, because the calculation of the stiffness matrices requires a numerical integration over each element in the mesh to impose the constraint (3.24). To overcome that difficulty, one may find more attractive (though requiring more analytical work) to calculate the coefficients in the tying expressions explicitly, and solve a relatively small system of linear equations for each element.

3.2.5 Other elements.

The MITC family of plate bending elements also includes a higher order 16-node quadrilateral element, MITC16, and two triangular elements, MITC7, and MITC12. All these elements have the same properties, namely, do not contain spurious modes (that is, satisfy the ellipticity condition), they are relatively insensitive to geometrical distortions, and do not lock for small thicknesses.

For the list of the elements we refer to [6], convergence results are presented in [9]; a mathematical analysis can be found, for example, in [18], [19], [45].

Chapter 4

Numerical analysis.

In this chapter we present an attempt of a numerical analysis of plate bending elements, based on RM theory, using procedures, similar to the inf-sup test, proposed for the problems of incompressible elasticity in [20], and for beam bending elements, based on Timoshenko beam theory in [6].

4.1 Matrix computations.

This section deals with simple matrix operations, inequalities, and eigenproblems, which we will need for the further analysis. Although these results are quite trivial and well-known, we still show all the derivations, to provide a general framework for managing problems of the inf-sup kind. For a deeper insight into the matrix computations issue we refer to [6] and [25], while a review of the properties of linear operators, as well as main spectral decompositions theorems, can be found in [38].

4.1.1 Eigenvalue decompositions. Generalized eigenvalue problems.

In the following considerations, all real-valued matrices appear in boldface, e.g., $\mathbf{A} \in \mathbb{R}^n \times \mathbb{R}^m$ is an n -by- m real valued matrix. Matrices represent perfect examples of closed range linear transformations, and thus, a-priori are quite easy to deal with. Let us take $m = n$ for the matrix \mathbf{A} introduced above; in the further analysis, we will concentrate on the symmetric matrices and assume $\mathbf{A} = \mathbf{A}^T$ by default, unless explicitly stated otherwise. Consider now the *standard eigenvalue problem*, associated with \mathbf{A} :

$$\begin{aligned} & \text{Find a set of eigenvalues } \lambda_i \text{ and eigenvectors } \underline{\phi}_i, \text{ such that} \\ & \mathbf{A}\underline{\phi}_i = \lambda_i\underline{\phi}_i, \quad i = 1..n; \quad \mathbf{\Phi}^T\mathbf{\Phi} = \mathbf{I}, \end{aligned} \tag{4.1}$$

where $\mathbf{\Phi} = \{\underline{\phi}_1, \dots, \underline{\phi}_n\}$, and \mathbf{I} is the n -by- n identity matrix. We can rewrite equivalently the eigenproblem (4.1) using matrix notation as

$$\text{Find matrices } \mathbf{\Lambda} \text{ and } \mathbf{\Phi}, \text{ such that } \mathbf{A}\mathbf{\Phi} = \mathbf{\Phi}\mathbf{\Lambda}, \quad \mathbf{\Phi}^T\mathbf{\Phi} = \mathbf{I},$$

where $\mathbf{\Lambda} = \text{diag}(\lambda_1, \dots, \lambda_n)$. Using the orthogonality of $\mathbf{\Phi}$ (i.e., $\mathbf{\Phi}^{-1} = \mathbf{\Phi}^T$), we obtain the *eigenvalue (or spectral) decomposition* of \mathbf{A} : $\mathbf{A} = \mathbf{\Phi}\mathbf{\Lambda}\mathbf{\Phi}^T$, or $\mathbf{\Phi}^T\mathbf{A}\mathbf{\Phi} = \mathbf{\Lambda}$.

Putting a positive definite matrix $\mathbf{B} \in \mathbb{R}^n \times \mathbb{R}^n$ on the l.h.s. of (4.1), we arrive at the *generalized eigenvalue problem*, namely

$$\begin{aligned} & \text{Find a set of eigenvalues } \lambda_i \text{ and eigenvectors } \underline{\phi}_i, \text{ such that} \\ & \mathbf{A}\underline{\phi}_i = \lambda_i\mathbf{B}\underline{\phi}_i, \quad i = 1..n; \quad \mathbf{\Phi}^T\mathbf{B}\mathbf{\Phi} = \mathbf{I}, \end{aligned}$$

or, in the matrix form,

$$\text{Find matrices } \mathbf{\Lambda} \text{ and } \mathbf{\Phi}, \text{ such that } \mathbf{A}\mathbf{\Phi} = \mathbf{B}\mathbf{\Phi}\mathbf{\Lambda}, \mathbf{\Phi}^T\mathbf{B}\mathbf{\Phi} = \mathbf{I}. \quad (4.2)$$

Multiplying both sides of (4.2) by $\mathbf{\Phi}^T$ on the left, we obtain that $\mathbf{\Phi}^T\mathbf{A}\mathbf{\Phi} = \mathbf{\Lambda}$, as it was before, in the standard case.

For the sake of simplicity, let us define a convenient notation for a generalized eigenproblem with a symmetric real-valued matrix \mathbf{A} , and symmetric positive definite r.h.s. matrix \mathbf{B} , as $GEP(\mathbf{A}, \mathbf{B})$.

Remark. We can clearly use all the concepts of functional spaces, studied in Chapter 2 for the matrix analysis. In particular, for two general vectors $\mathbf{V} = [v_1, \dots, v_n]^T \in \mathcal{V} = \mathbb{R}^n \times \mathbb{R}^1$ and $\mathbf{W} = [w_1, \dots, w_n] \in \mathcal{W} = (\mathcal{V})' = \mathbb{R}^1 \times \mathbb{R}^n$, we will use a duality pairing between the spaces as follows: $\langle \mathbf{W}, \mathbf{V} \rangle = \mathbf{W}\mathbf{V} = \sum_{i=1}^n w_i v_i$. \square

4.1.2 Vector and matrix norms. Basic inequalities.

For a real valued vector $\mathbf{V} = [v_1, \dots, v_n]^T \in \mathbb{R}^n \times \mathbb{R}^1$, and a general real-valued matrix $\mathbf{A} \in \mathbb{R}^n \times \mathbb{R}^m$, we define the following norms, as given in [6]:

$$\|\mathbf{V}\|_2^2 = \langle \mathbf{V}^T, \mathbf{V} \rangle, \quad \|\mathbf{A}\|_2^2 = \lambda_{\max}, \quad (4.3)$$

where λ_{\max} is the largest eigenvalue of the matrix $\mathbf{A}^T\mathbf{A}$. Let us also define a vector seminorm

$$|\mathbf{V}|_{\mathbf{B}}^2 = \langle \mathbf{V}^T, \mathbf{B}\mathbf{V} \rangle, \quad (4.4)$$

where \mathbf{B} is a symmetric, real-valued, positive semidefinite n -by- n matrix. If $Ker(\mathbf{B}) = \underline{0}$ (i.e., \mathbf{B} is positive definite rather than semidefinite), then this seminorm becomes a norm, equivalent to (4.3) for all \mathbf{V} in $\mathbb{R}^n \times \mathbb{R}^1$. If, however, the null space of \mathbf{B} is not trivial, then the equivalence of (4.4) to (4.3) holds only

on the subspace $\mathcal{D} = [\mathbb{R}^n \times \mathbb{R}^1] \setminus Ker(\mathbf{B})$. Let us explicitly show this result in the following proposition.

Proposition 5. $|\mathbf{V}|_{\mathbf{B}}$ is equivalent to $\|\mathbf{V}\|_2 \forall \mathbf{V} \in \mathcal{D}$.

Proof. We need to show that there exist two positive constants c_1 and c_2 , such that

$$c_1 \|\mathbf{V}\|_2 \leq |\mathbf{V}|_{\mathbf{B}} \leq c_2 \|\mathbf{V}\|_2 \quad \forall \mathbf{V} \in \mathcal{D}. \quad (4.5)$$

Let us rewrite $\mathbf{V} = \Phi \tilde{\mathbf{V}}$, where Λ and Φ are the eigenvalues and eigenvectors of the standard eigenproblem associated with \mathbf{B} . Then

$$\begin{aligned} |\mathbf{V}|_{\mathbf{B}}^2 &= \langle \mathbf{V}^T, \mathbf{B}\mathbf{V} \rangle = \langle \tilde{\mathbf{V}}^T \Phi^T, \mathbf{B}\Phi \tilde{\mathbf{V}} \rangle \stackrel{\text{use } \Phi^T \mathbf{B} \Phi = \Lambda}{=} \langle \tilde{\mathbf{V}}^T, \Lambda \tilde{\mathbf{V}} \rangle \stackrel{\text{use } \tilde{\mathbf{V}} = \Phi^T \mathbf{V} \text{ and } \Phi^T \Phi = \mathbf{I}}{=} \\ &= \sum_{i=1}^n \lambda_i v_i^2 \stackrel{\text{use } \mathbf{V} \in \mathcal{D}}{=} \sum_{i=m+1}^n \lambda_i v_i^2, \end{aligned}$$

where m is the dimension of the null space of matrix \mathbf{B} (and the number of corresponding zero eigenvalues, $\lambda_i = 0, i = 1..m$). Therefore, we have that

$$\lambda_{\min} \sum_{i=1}^n v_i^2 \leq |\mathbf{V}|_{\mathbf{B}}^2 \leq \lambda_{\max} \sum_{i=1}^n v_i^2,$$

where λ_{\min} and λ_{\max} stand for the smallest nonzero and the greatest eigenvalues of the $GEP(\mathbf{B}, \mathbf{I})$ correspondingly. Of course, this result is nothing else, but the celebrated *Rayleigh quotient* [6]. Recalling that $\|\mathbf{V}\|_2^2 = \sum_{i=1}^n v_i^2$, we conclude that (4.5) holds with $c_1 = \sqrt{\lambda_{\min}}$ and $c_2 = \sqrt{\lambda_{\max}}$. \square

Remark. The result of Proposition 5 certainly holds in the "trivial" case, when $Ker(\mathbf{B}) = \mathbf{0}$ (or $\mathcal{D} = \mathbb{R}^n \times \mathbb{R}^1$). \square

Another important vector inequality, which will be extensively used, is the *Cauchy-Schwarz inequality for real numbers* [38]:

If v_1, v_2, \dots, v_n and w_1, w_2, \dots, w_n are real numbers, then

$$\left(\sum_{i=1}^n v_i w_i \right)^2 \leq \left(\sum_{i=1}^n v_i^2 \right) \left(\sum_{i=1}^n w_i^2 \right). \quad (4.6)$$

We can rewrite the above inequality in terms of vector norms as: $\|\langle \mathbf{V}, \mathbf{W} \rangle\|_2^2 \leq \|\mathbf{V}\|_2^2 \|\mathbf{W}\|_2^2$. Let us note that the sufficient condition to get the equality is: $v_i = w_i, i = 1..n$.

4.2 Analysis of the inf-sup condition.

Here we present a discussion of the numerical analysis of the *inf-sup condition* in the Γ'_h -norm, given by equation (3.3). The proposed numerical procedures for evaluating the performance of the elements are similar to the inf-sup test [20]; for a related analysis of a number of eigenproblems of the inf-sup type that appear in the incompressible media analysis, we refer to [34].

4.2.1 Matrix form of the inf-sup condition in the Γ'_h -norm.

This, and the following two sections, concentrate on the numerical treatment of the discrete inf-sup condition in the Γ'_h -norm, given by (3.19).

We choose the following norm over the space for rotations and transverse displacement (restricting our analysis to the case of bounded domains):

$$\begin{aligned} \|\underline{v}_h\|_V^2 &= \|\underline{v}_h\|_{H^1(\Omega)}^2 \stackrel{\text{by (2.3)}}{\simeq} |\underline{v}_h|_{H^1(\Omega)}^2 = |\underline{\eta}_h|_{H^1(\Omega)}^2 + |\xi_h|_{H^1(\Omega)}^2 = \\ &= L^2 \sum_{i,j=1}^2 \|\eta_{hi,j}\|_{L^2(\Omega)}^2 + \sum_{i=1}^2 \|\xi_{h,i}\|_{L^2(\Omega)}^2 = \mathbf{V}^T \mathbf{S} \mathbf{V} = \|\mathbf{V}\|_{\mathbf{S}}^2, \end{aligned}$$

where L is a characteristic dimension of the plate (e.g., plate's length or width),

$\mathbf{V} \in \mathbb{R}^n$ is a vector of nodal point displacements, and $\mathbf{S} \in \mathbb{R}^n \times \mathbb{R}^n$ is a positive definite norm matrix.

Shear strains are calculated from nodal point displacements \mathbf{V} using a shear nodal basis $\mathbf{B}_\gamma : \mathbb{R}^n \rightarrow \Gamma_h$, as $\underline{\gamma}_h = \mathbf{B}_\gamma \mathbf{V}$. Let us define the L^2 -inner product of \mathbf{B}_γ 's as $\mathbf{G} = (\mathbf{B}_\gamma^T, \mathbf{B}_\gamma) \in \mathbb{R}^n \times \mathbb{R}^n$; then the bilinear form in the numerator of the inf-sup condition can be rewritten as $(\underline{\gamma}_h, \underline{\chi}_h) = (\mathbf{U}^T \mathbf{B}_\gamma^T, \mathbf{B}_\gamma \mathbf{V}) = \mathbf{U}^T \mathbf{G} \mathbf{V}$, where \mathbf{G} is a positive semidefinite n -by- n matrix. To avoid corner solutions (i.e., the inf-sup value being zero or infinity), we have to impose the following restriction: $\mathbf{V}, \mathbf{U} \in \mathcal{D} = \mathbb{R}^n \setminus \text{Ker}(\mathbf{G})$. Summarizing, we can deduce the matrix representation of the discrete inf-sup condition in the Γ'_h -norm (3.19):

$$\inf_{\mathbf{U} \in \mathcal{D}} \sup_{\mathbf{V} \in \mathcal{D}} \frac{\mathbf{U}^T \mathbf{G} \mathbf{V}}{\|\mathbf{B}_\gamma \mathbf{U}\|_{\Gamma'_h} \|\mathbf{V}\|_{\mathbf{S}}} \geq \beta > 0 \quad (4.7)$$

4.2.2 Discrete inf-sup condition in the L^2 -norm.

As we have shown in Section 2.4.1, for the case of zero plate thickness, $t = 0$, $L^2(\Omega)$ is not the appropriate space for shears, i.e., the norm of shears in $L^2(\Omega)$ is not bounded from above. The purpose of this section is to show that this result can be demonstrated and confirmed by a simple numerical experiment.

Let us assume that the appropriate space for shears in case of zero thickness is $L^2(\Omega)$, therefore the corresponding norm is given by $\|\underline{\gamma}_h\|_{\Gamma'_h} = \|\underline{\gamma}_h\|_{L^2(\Omega)} = \|\mathbf{B}_\gamma \mathbf{U}\|_{L^2(\Omega)} = \sqrt{(\mathbf{U}^T \mathbf{B}_\gamma^T, \mathbf{B}_\gamma \mathbf{U})} = |\mathbf{U}|_{\mathbf{G}}$.

The inf-sup condition has the form:

$$\inf_{\mathbf{U} \in \mathcal{D}} \sup_{\mathbf{V} \in \mathcal{D}} \frac{\mathbf{U}^T \mathbf{G} \mathbf{V}}{|\mathbf{U}|_{\mathbf{G}} \|\mathbf{V}\|_{\mathbf{S}}} \geq \beta \quad (4.8)$$

with the inf sup value $\beta = \sqrt{\lambda_{\min}}$, where λ_{\min} stands for a smallest nonzero eigenvalue of the $GEP(\mathbf{G}, \mathbf{S})$ (see Example 4.41 in [6] for the derivation).

To check the performance of the elements, we apply the inf-sup test proce-

ture to a simple problem (see Fig. 4-1), using quadrilateral displacement-based elements (QUAD's) as well as the elements of the MITC family.

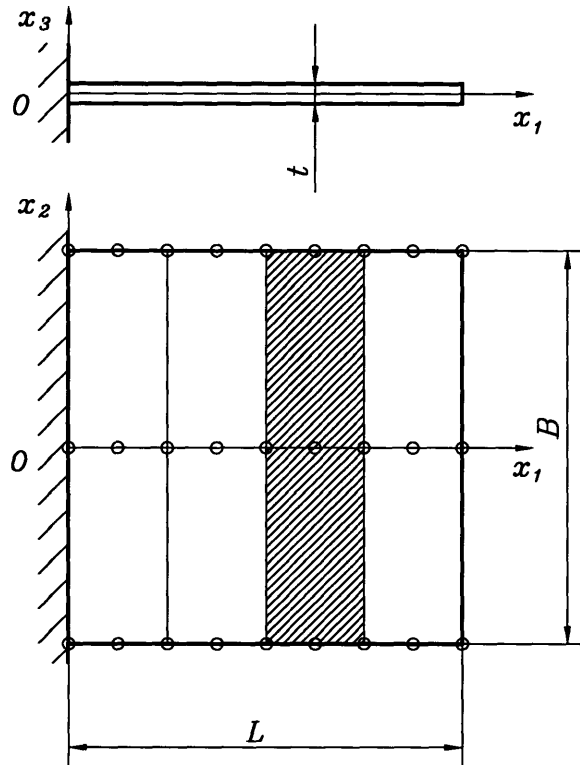


Figure 4-1: Cantilever plate considered in the inf-sup test. Top view shows a typical mesh of four none-node elements.

We expect that, due to the unbounded growth of the $\|\underline{\gamma}_h\|_{L^2(\Omega)}$ term in the denominator of (4.8), the inf-sup value β will go to zero. If we find that for some element, the inf-sup curve escapes this trend, then our theoretical prediction that $L^2(\Omega)$ is not the correct space for shears will be contradicted.

Numerical results of the test are shown in Fig. 4-2 for the case $L = B = 100$.

All curves in the figure demonstrate that the discrete inf-sup value β converges to zero with a linear rate, which does not contradict the analytical results.

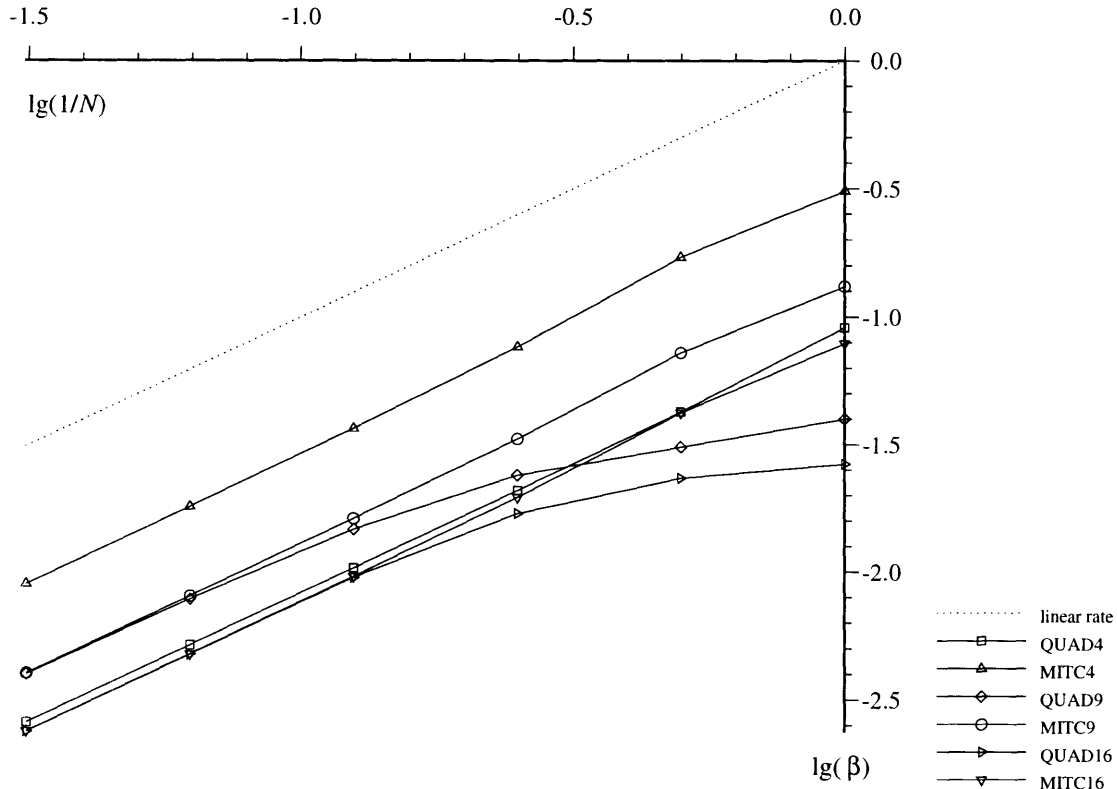


Figure 4-2: Inf-sup test of plate bending elements in the L^2 -norm (cantilever plate).

4.2.3 Inf-sup test in the Γ'_h -norm.

Let us obtain the expression for the inf-sup value when we use the appropriate space for shears with a dual discrete norm given by equation (3.20).

We take

$$\|\underline{\chi}_h\|_{\Gamma_h}^2 = \|\underline{\chi}_h\|_{L^2(\Omega)}^2 + L^2 \|\text{rot } \underline{\chi}_h\|_{L^2(\Omega)}^2 = \mathbf{V}^T (\mathbf{G} + \mathbf{Q}) \mathbf{V} = \mathbf{V}^T \mathbf{D} \mathbf{V} \stackrel{\mathbf{V} \in \mathcal{D}}{=} |\mathbf{V}|_{\mathbf{D}}^2,$$

where \mathbf{D} is a positive semidefinite matrix, and L is a characteristic dimension of the plate. Note that the condition $\mathbf{V} \in \mathcal{D}$ is sufficient to guarantee

$\mathbf{V} \notin \text{Ker}(\mathbf{D})$ ($\mathbf{V}^T \mathbf{G} \mathbf{V} > 0 \forall \mathbf{V} \in \mathcal{D}$, and since \mathbf{Q} is a positive semidefinite matrix, $\mathbf{V}^T \mathbf{Q} \mathbf{V} \geq 0 \forall \mathbf{V} \in \mathbb{R}^n$; therefore $\mathbf{V}^T (\mathbf{G} + \mathbf{Q}) \mathbf{V} > 0 \forall \mathbf{V} \in \mathcal{D}$). Then

$$\begin{aligned} \|\underline{\gamma}_h\|_{\Gamma'_h} &= \|\mathbf{B}_\gamma \mathbf{U}\|_{\Gamma'_h} \stackrel{\text{use (3.20)}}{=} \sup_{\mathbf{V} \in \mathcal{D}} \frac{(\mathbf{V}^T \mathbf{B}_\gamma^T, \mathbf{B}_\gamma \mathbf{U})}{|\mathbf{V}|_{\mathbf{D}}} = \sup_{\mathbf{V} \in \mathcal{D}} \frac{\mathbf{V}^T \mathbf{G} \mathbf{U}}{|\mathbf{V}|_{\mathbf{D}}} \stackrel{\text{by (4.5)}}{\leq} \\ &\leq \sup_{\mathbf{V} \in \mathcal{D}} \frac{\mathbf{V}^T \mathbf{G} \mathbf{U}}{\sqrt{\delta_{\min}} \|\mathbf{V}\|_2} \stackrel{\text{use (4.6)}}{=} \frac{\|\mathbf{G} \mathbf{U}\|_2}{\sqrt{\delta_{\min}}}, \end{aligned} \quad (4.9)$$

where δ_{\min} stands for the smallest nonzero eigenvalue of \mathbf{D} . Moreover, by (4.5) we have:

$$\|\mathbf{V}\|_{\mathbf{S}} \leq \sqrt{\sigma_{\max}} \|\mathbf{V}\|_2, \quad (4.10)$$

where σ_{\max} is the largest eigenvalue of \mathbf{S} .

Substituting (4.9) and (4.10) into equation (4.7), we obtain

$$\begin{aligned} \inf_{\mathbf{U} \in \mathcal{D}} \sup_{\mathbf{V} \in \mathcal{D}} \frac{\mathbf{U}^T \mathbf{G} \mathbf{V}}{\|\mathbf{B}_\gamma \mathbf{U}\|_{\Gamma'_h} \|\mathbf{V}\|_{\mathbf{S}}} &\geq \sqrt{\frac{\delta_{\min}}{\sigma_{\max}}} \inf_{\mathbf{U} \in \mathcal{D}} \sup_{\mathbf{V} \in \mathcal{D}} \frac{\mathbf{U}^T \mathbf{G} \mathbf{V}}{\|\mathbf{G} \mathbf{U}\|_2 \|\mathbf{V}\|_2} \stackrel{\text{use (4.6)}}{=} \\ &= \sqrt{\frac{\delta_{\min}}{\sigma_{\max}}} \inf_{\mathbf{U} \in \mathcal{D}} \frac{\|\mathbf{G} \mathbf{U}\|_2}{\|\mathbf{G} \mathbf{U}\|_2} \stackrel{\text{use } \mathbf{U} \in \mathcal{D}}{=} \sqrt{\frac{\delta_{\min}}{\sigma_{\max}}} = \beta. \end{aligned} \quad (4.11)$$

Now we can apply the same procedure to study convergence of the discrete inf-sup value β ¹. Results of the test for four- and nine-node quadrilateral plate bending elements are shown in Fig. 4-3.

The β of the four-node quadrilateral displacement-based element QUAD4 converges to zero, confirming the locking properties of the element demonstrated in Appendix A. Other elements do not show that trend, which also agrees with numerical simulations; therefore we conclude that the QUAD9, MITC4 and MITC9 elements have passed the inf-sup test in the Γ'_h -norm.

Let us emphasize that these results do not pretend to prove that we satisfy either the inf-sup condition (3.3), or (3.19) for every problem and every mesh

¹Another, though computationally less efficient way of calculating the inf-sup value β is presented in Appendix B.

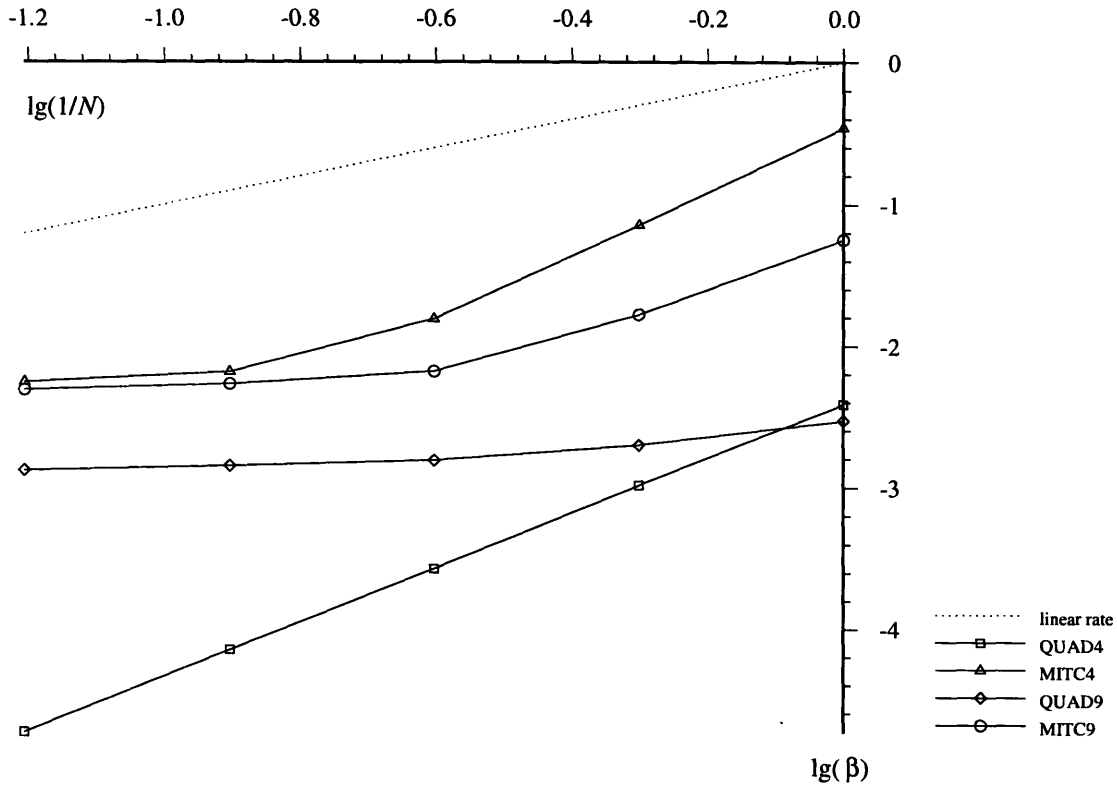


Figure 4-3: Inf-sup test of the plate elements in the Γ'_h -norm (cantilever plate).

sequence; they are certainly limited to the consideration of the particular demonstrative example, and weaker than the analytical results of Proposition 4. On the other hand, this routine allows us to test general FE meshes with distorted elements, for which we can barely extend the analytical results.

4.2.4 From Γ'_h to Γ' .

As we have demonstrated in Section 3.1.4, in order to prove that the discrete inf-sup condition (3.3) is satisfied for a given FEM discretization, we need to show that:

1. The discrete inf-sup condition holds with respect to Γ'_h -norm for shears, as given in (3.19)-(3.20);
2. The norm equivalence stated in (3.21) holds with a constant ρ independent of the mesh size and plate thickness.

The inf-sup test from the previous section enables us to check, whether the first condition is satisfied, while this section is devoted to a development of a similar numerical procedure, which will allow to check whether the latter holds for a given particular case.

Let us make a refinement of the FEM space with a characteristic mesh size h , simply subdividing every element onto four subelements, and call the resulting discrete FEM space for shears $\Gamma_{h/2}$. The next refinement will give us a space $\Gamma_{h/4}$, and so on. Clearly, we have that $\Gamma_h \subset \Gamma_{h/2} \subset \Gamma_{h/4} \dots \subset \Gamma_{h/2n} \subset \Gamma$. Therefore, choosing the number of refinements n , we can approach the continuous space Γ as closely as wanted by our FEM discretization².

Moreover, for $\underline{\gamma}_h \in \Gamma_h$ we have that

$$\|\underline{\gamma}_h\|_{\Gamma'_{h/2n}} = \sup_{\underline{x}_h \in \Gamma_{h/2n}, \underline{x}_h \neq 0} \frac{(\underline{x}_h, \underline{\gamma}_h)}{\|\underline{x}_h\|_{\Gamma_{h/2n}}} \text{ with } \lim_{n \rightarrow \infty} \|\underline{\gamma}_h\|_{\Gamma'_{h/2n}} = \|\underline{\gamma}_h\|_{\Gamma'}.$$

Thus, to check whether the norm equivalence (3.21) holds, we can look for a sequence of problems

$$\|\underline{\gamma}_h\|_{\Gamma'_h} = \rho_n \|\underline{\gamma}_h\|_{\Gamma'_{h/2n}}, \quad (4.12)$$

and trace the constant ρ_n as we increase n . If ρ_n does not converge to zero, we say that the test is passed, and, combining this with results of the inf-sup test in the Γ'_h -norm, we state that the inf-sup condition (3.3) is satisfied for a given discretization.

²To confirm this statement, we have to recall well-known convergence properties of the FEM discrete spaces; see, e.g., Section 4.3 of [6].

To find the worst case which is predicted by the theory, we will look for the greatest lower bound of ρ_n , given by

$$\rho_n = \inf_{\gamma_h \in \Gamma_h, \gamma_h \neq 0} \frac{\sup_{\bar{\chi}_h \in \Gamma_h, \bar{\chi}_h \neq 0} \frac{(\bar{\chi}_h, \gamma_h)}{\|\bar{\chi}_h\|_{\Gamma_h}}}{\sup_{\bar{\bar{\chi}}_h \in \Gamma_{h/2n}, \bar{\bar{\chi}}_h \neq 0} \frac{(\bar{\bar{\chi}}_h, \gamma_h)}{\|\bar{\bar{\chi}}_h\|_{\Gamma_{h/2n}}}}. \quad (4.13)$$

In order to rewrite the expression (4.13) in matrix form, we define:

$$\begin{aligned} \underline{\gamma}_h &= \bar{\mathbf{B}}_\gamma \mathbf{U}, & \underline{\chi}_h &= \bar{\mathbf{B}}_\gamma \bar{\mathbf{V}}, & \bar{\mathbf{B}}_\gamma: \mathbb{R}^{\bar{n}} &\rightarrow \Gamma_h; & \mathbf{U}, \bar{\mathbf{V}} &\in \mathbb{R}^{\bar{n}}; \\ \|\underline{\chi}_h\|_{\Gamma_h} &=_{\bar{\mathbf{V}} \in \bar{\mathcal{D}}} |\bar{\mathbf{V}}|_{\bar{\mathbf{D}}}, & \bar{\mathbf{G}} &= (\bar{\mathbf{B}}_\gamma^T, \bar{\mathbf{B}}_\gamma); & \bar{\mathbf{D}}, \bar{\mathbf{G}} &\in \mathbb{R}^{\bar{n}} \times \mathbb{R}^{\bar{n}}; \\ \bar{\underline{\chi}}_h &= \bar{\bar{\mathbf{B}}}_\gamma \bar{\bar{\mathbf{V}}}, & \bar{\bar{\mathbf{B}}}_\gamma: \mathbb{R}^{\bar{\bar{n}}} &\rightarrow \Gamma_{h/2n}; & \bar{\bar{\mathbf{G}}} &= (\bar{\bar{\mathbf{B}}}_\gamma^T, \bar{\bar{\mathbf{B}}}_\gamma); \\ \|\bar{\underline{\chi}}_h\|_{\Gamma_{h/2n}} &=_{\bar{\bar{\mathbf{V}}} \in \bar{\bar{\mathcal{D}}}} |\bar{\bar{\mathbf{V}}}|_{\bar{\bar{\mathbf{D}}}}, & \bar{\bar{\mathbf{D}}} &\in \mathbb{R}^{\bar{\bar{n}}} \times \mathbb{R}^{\bar{\bar{n}}}; & \bar{\bar{\mathbf{G}}} &= (\bar{\bar{\mathbf{B}}}_\gamma^T, \bar{\bar{\mathbf{B}}}_\gamma); & \bar{\bar{\mathbf{G}}} &\in \mathbb{R}^{\bar{\bar{n}}} \times \mathbb{R}^{\bar{\bar{n}}}, \end{aligned} \quad (4.14)$$

where \bar{n} is the dimension of the discrete space Γ_h , and $\bar{\bar{n}}$ stands for the dimension of $\Gamma_{h/2n}$. Substituting (4.14) into equation (4.13), and defining the corresponding domains $\bar{\mathcal{D}} = \mathbb{R}^{\bar{n}} \setminus \text{Ker}(\bar{\mathbf{G}})$ and $\bar{\bar{\mathcal{D}}} = \mathbb{R}^{\bar{\bar{n}}} \setminus \text{Ker}(\bar{\bar{\mathbf{G}}})$ to escape from the trivial answer, we obtain

$$\rho_n = \inf_{\mathbf{U} \in \bar{\mathcal{D}}} \frac{\sup_{\bar{\mathbf{V}} \in \bar{\mathcal{D}}} \frac{\bar{\mathbf{V}}^T \bar{\mathbf{G}} \mathbf{U}}{|\bar{\mathbf{V}}|_{\bar{\mathbf{D}}}}}{\sup_{\bar{\bar{\mathbf{V}}} \in \bar{\bar{\mathcal{D}}}} \frac{\bar{\bar{\mathbf{V}}}^T \bar{\bar{\mathbf{G}}} \mathbf{U}}{|\bar{\bar{\mathbf{V}}}|_{\bar{\bar{\mathbf{D}}}}}}. \quad (4.15)$$

To calculate the greatest lower bound of ρ_n , we have to find a lower bound for the expression in the numerator, and an upper bound for the denominator in (4.15).

$$\sup_{\bar{\mathbf{V}} \in \bar{\mathcal{D}}} \frac{\bar{\mathbf{V}}^T \bar{\mathbf{G}} \mathbf{U}}{\|\bar{\mathbf{V}}\|_{\bar{\mathbf{D}}}} \stackrel{\text{by (4.5)}}{\geq} \frac{1}{\sqrt{\bar{\delta}_{\max}}} \sup_{\bar{\mathbf{V}} \in \bar{\mathcal{D}}} \frac{\bar{\mathbf{V}}^T \bar{\mathbf{G}} \mathbf{U}}{\|\bar{\mathbf{V}}\|_2} \stackrel{\text{use (4.6) with } \bar{\mathbf{V}} = \bar{\mathbf{G}} \mathbf{U}}{=} \frac{1}{\sqrt{\bar{\delta}_{\max}}} \|\bar{\mathbf{G}} \mathbf{U}\|_2; \quad (4.16)$$

$$\sup_{\bar{\mathbf{V}} \in \bar{\mathcal{D}}} \frac{\bar{\mathbf{V}}^T \tilde{\mathbf{G}} \mathbf{U}}{\|\bar{\mathbf{V}}\|_{\bar{\mathbf{D}}}} \stackrel{\text{by (4.5)}}{\leq} \frac{1}{\sqrt{\bar{\delta}_{\min}}} \sup_{\bar{\mathbf{V}} \in \bar{\mathcal{D}}} \frac{\bar{\mathbf{V}}^T \tilde{\mathbf{G}} \mathbf{U}}{\|\bar{\mathbf{V}}\|_2} \stackrel{\text{use (4.6) with } \bar{\mathbf{V}} = \tilde{\mathbf{G}} \mathbf{U}}{=} \frac{1}{\sqrt{\bar{\delta}_{\min}}} \|\tilde{\mathbf{G}} \mathbf{U}\|_2, \quad (4.17)$$

where $\bar{\delta}_{\max}$ is the maximal eigenvalue of matrix $\bar{\mathbf{D}}$, and $\bar{\delta}_{\min}$ stands for the smallest nonzero eigenvalue of $\bar{\mathbf{D}}$.

Substituting (4.16) and (4.17) into (4.15), we obtain the greatest lower bound for $\underline{\rho}_n$ as:

$$\begin{aligned} \underline{\rho}_n &\geq \sqrt{\frac{\bar{\delta}_{\min}}{\bar{\delta}_{\max}}} \inf_{\mathbf{U} \in \bar{\mathcal{D}}} \frac{\|\bar{\mathbf{G}} \mathbf{U}\|_2}{\|\tilde{\mathbf{G}} \mathbf{U}\|_2} = \sqrt{\frac{\bar{\delta}_{\min}}{\bar{\delta}_{\max}}} \inf_{\mathbf{U} \in \bar{\mathcal{D}}} \left[\frac{\|\bar{\mathbf{G}} \mathbf{U}\|_2}{\|\mathbf{U}\|_2} \frac{\|\mathbf{U}\|_2}{\|\tilde{\mathbf{G}} \mathbf{U}\|_2} \right] = \\ &= \sqrt{\frac{\bar{\delta}_{\min}}{\bar{\delta}_{\max}}} \frac{\inf_{\mathbf{U} \in \bar{\mathcal{D}}} \frac{\|\bar{\mathbf{G}} \mathbf{U}\|_2}{\|\mathbf{U}\|_2}}{\sup_{\mathbf{U} \in \bar{\mathcal{D}}} \frac{\|\tilde{\mathbf{G}} \mathbf{U}\|_2}{\|\mathbf{U}\|_2}} \stackrel{\text{set } \|\mathbf{U}\|_2 = 1}{=} \frac{\sqrt{\bar{\delta}_{\min}} \bar{\gamma}_{\min}}{\sqrt{\bar{\delta}_{\max}} \vartheta_{\max}} = \delta_n, \end{aligned} \quad (4.18)$$

with $\bar{\gamma}_{\min}$ being the smallest nonzero eigenvalue of $\bar{\mathbf{G}}$, and ϑ_{\max} the greatest eigenvalue of a matrix $\mathbf{T} = \tilde{\mathbf{G}}^T \tilde{\mathbf{G}}$. Therefore, we can apply a numerical procedure, similar to the inf-sup test to trace the value δ_n as we increase n^3 .

Results of the test for the displacement-based and MITC four- and nine-node elements are presented in Fig. 4-4. We can clearly see that the QUAD4's δ_n monotonically converges to zero as we increase the dimension of the trial space $\Gamma_{h/2n}$. Therefore, we state that the constant ρ_n for QUAD4 is not bounded from

³Since $\bar{\gamma}_{\min}$ and $\bar{\delta}_{\max}$ do not change with n , there is no need to recalculate them; they should be calculated only in the original space Γ'_h . Also, we note that the dimension of the eigenproblem for ϑ_{\max} , \bar{n} , corresponds to the dimension of the smallest space Γ'_h . Therefore, the only expensive calculation (i.e., an eigenproblem of size \bar{n}) is required to get the eigenvalue $\bar{\delta}_{\min}$.

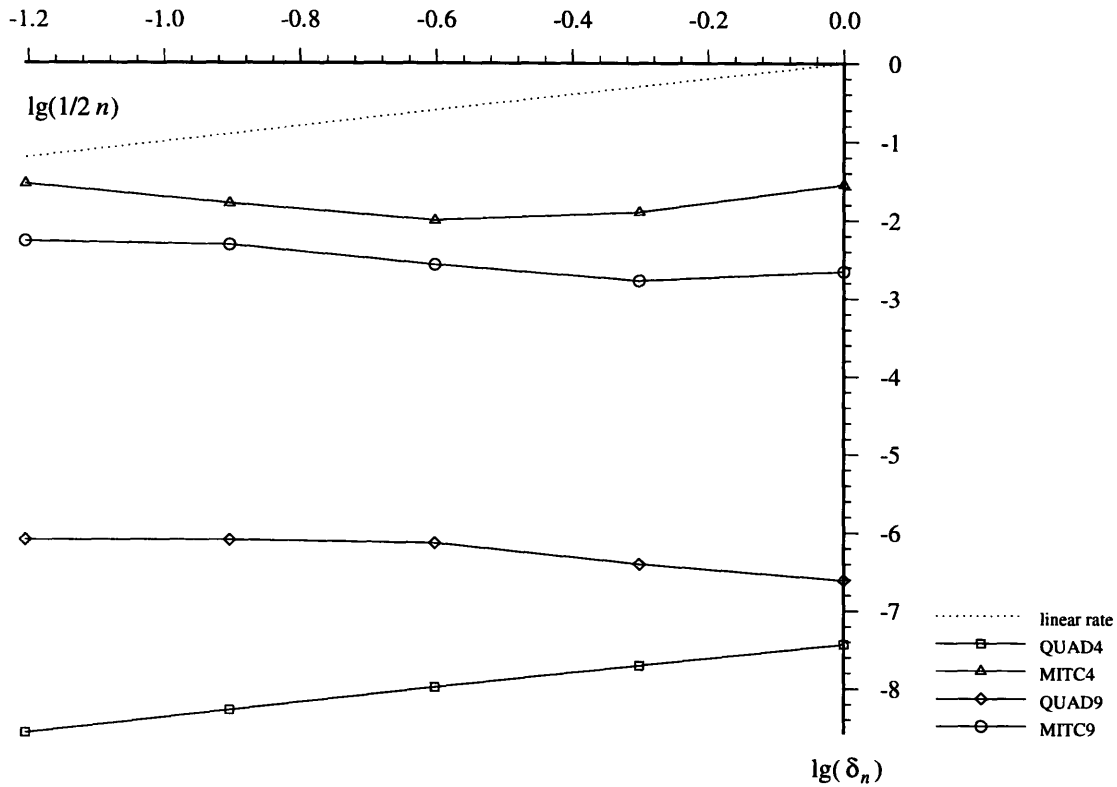


Figure 4-4: Behavior of δ_n for quadrilateral plate bending elements (cantilever plate).

below, and the test is failed. The other elements do not exhibit this trend; the corresponding curves for δ_n do not go down as we make refinements of Γ_h ; this allows us to manifest that for a given particular problem we will be able to find a finite nontrivial lower bound for the constant ρ_n as n goes to infinity, and thus, the discrete norm equivalence (4.12) holds with ρ_n independent of n . Because the plate's thickness does not show up in the expression (4.18), the constant ρ_n also does not depend on t . Convergence properties of the discrete FEM spaces allow us to extend this result to the "continuous world", and state that the norm equivalence (3.21) holds for a given problem with a constant ρ independent of

the plate thickness.

Summarizing, we are able to conclude that for the problem under consideration, the QUAD4 element does not satisfy the inf-sup condition, locks for a broad range of plate thicknesses, while the mixed interpolated elements and the QUAD9 element pass the developed inf-sup test, and do not lock. These results are confirmed by numerical simulations shown in Appendix A.

4.3 Numerical results.

This section presents an analysis of the problem, which is known to be the most severe test for the locking behavior. We will consider a clamped square plate (see Fig. 4-5), with $L = B = 100\text{ mm}$, and study the robustness of quadrilateral plate bending elements to changes in thickness and mesh distortions.

Following the procedure developed in the previous sections, we firstly run the two tests, given by equations (4.11) and (4.18), for a sequence of uniform meshes, shown in Fig. 4-6.

The results are basically the same as they were for the cantilever plate case: the QUAD4 element locks, while the QUAD9 and the mixed-interpolated elements produce good results, and do not lock for small thickness/length ratios. Fig. 4-7 demonstrates the numerical results of the inf-sup test in the Γ'_h -norm, while Fig. 4-8 shows the results of the δ_n -test.

Since for this case the results from the two tests seem to be perfectly correlated⁴, we can conclude that the rate of change of the smallest eigenvalue of the norm matrix \mathbf{D} , (referred to as δ_{\min} in (4.11) and as $\bar{\delta}_{\min}$ in (4.18)) dominates the qualitative behavior of the elements for the particular problem under consideration. Therefore, without loss of generality, we will further run only the inf-sup test in the Γ'_h -norm for the same problem and the same set of elements, using slightly

⁴I.e., the simulations show that if an element fails the inf-sup test in Γ'_h -norm, it does not pass the δ_n -test either, and visa versa.

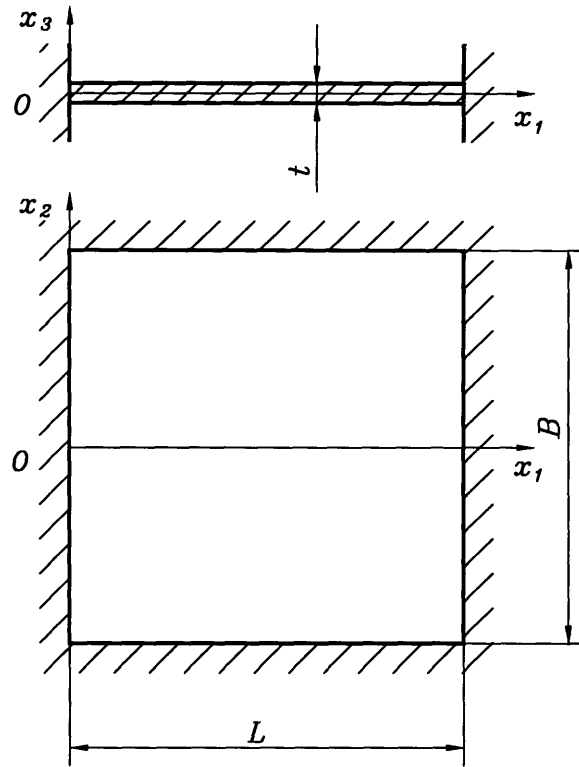


Figure 4-5: Clamped plate.

distorted meshes, as shown in Fig. 4-9⁵.

The results of the test are presented in Fig. 4-10. One can see that for this case both displacement-based elements "collapsed"; the corresponding lines for the QUAD4 and QUAD9 elements converge to zero. The mixed-interpolated elements, MITC4 and MITC9, passed the test, displaying their robustness to mesh distortions and changes in thickness.

Appendix A presents the numerical evidence, absolutely consistent with our results, thus justifying the proposed testing methodology.

⁵The meshes were chosen to preserve the "conforming" properties of the FE spaces, i.e., (A) \subset (B) \subset (C) \subset (D), which implies $V_h \subset V_{h/2} \subset V_{h/4} \subset V_{h/8}$.

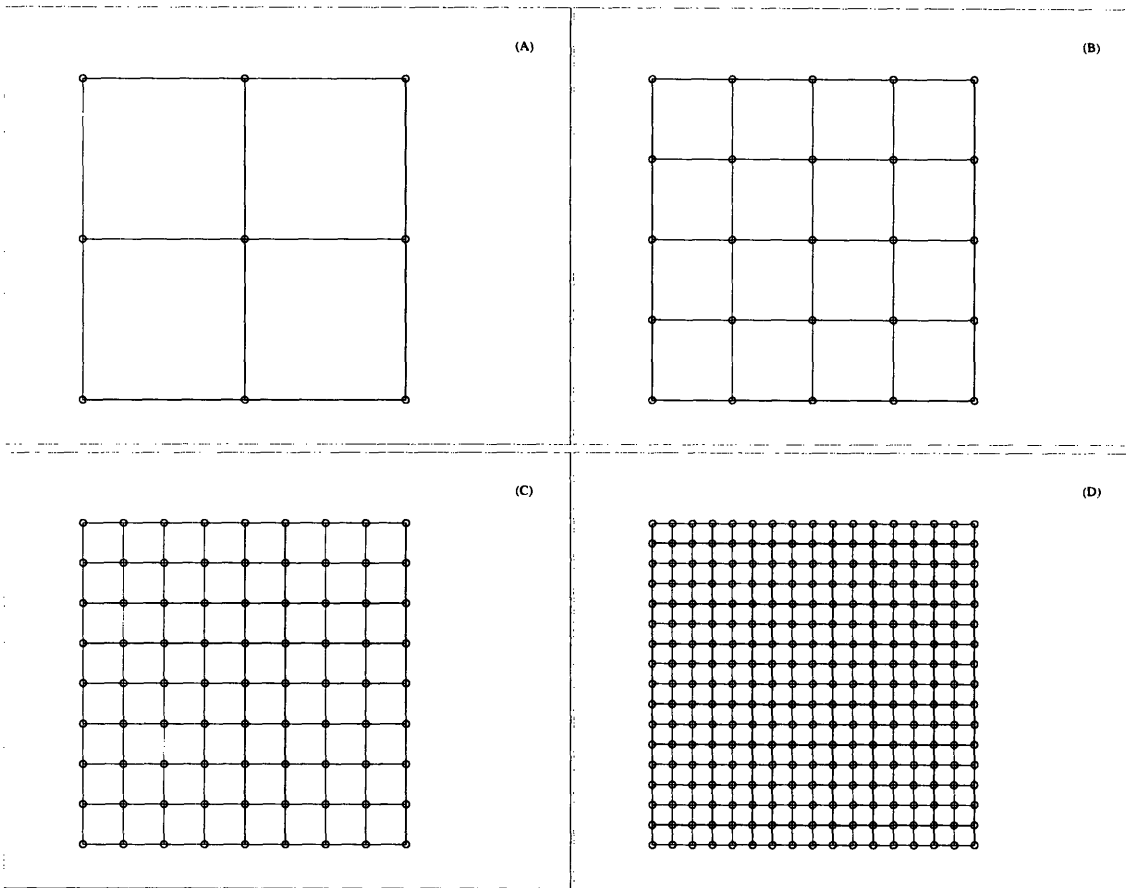


Figure 4-6: Uniform meshes used for the inf-sup test of the clamped plate case.

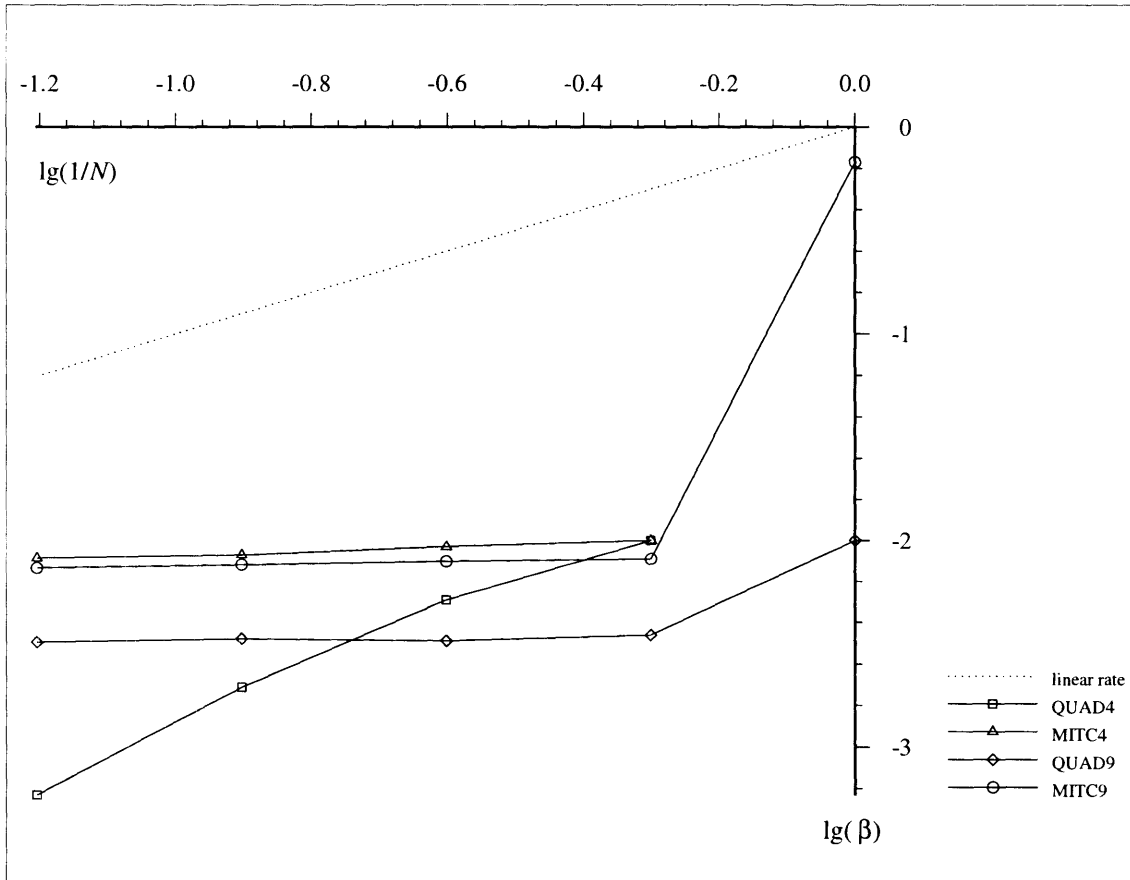


Figure 4-7: Inf-sup test of the quadrilateral plate bending elements in the Γ'_h -norm (clamped plate case, uniform meshes).

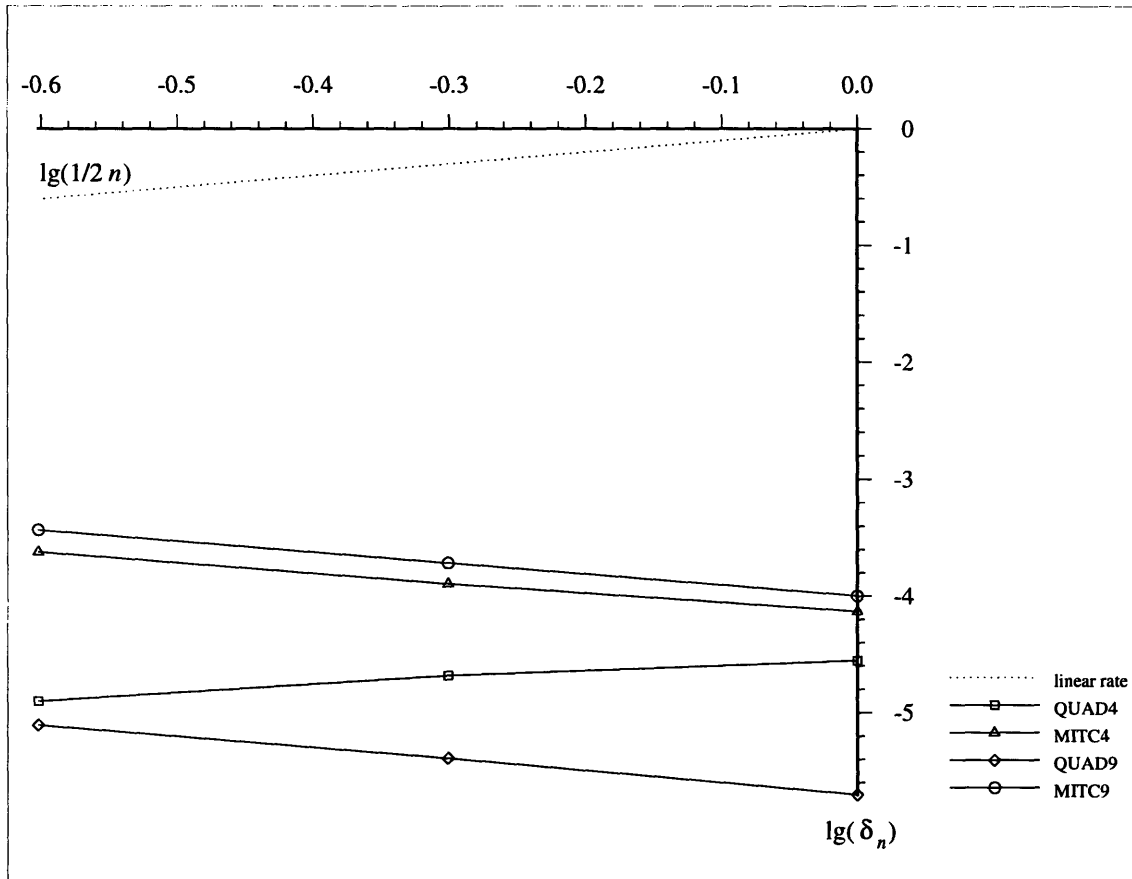


Figure 4-8: δ_n -test of the quadrilateral plate bending elements (clamped plate case, uniform meshes).

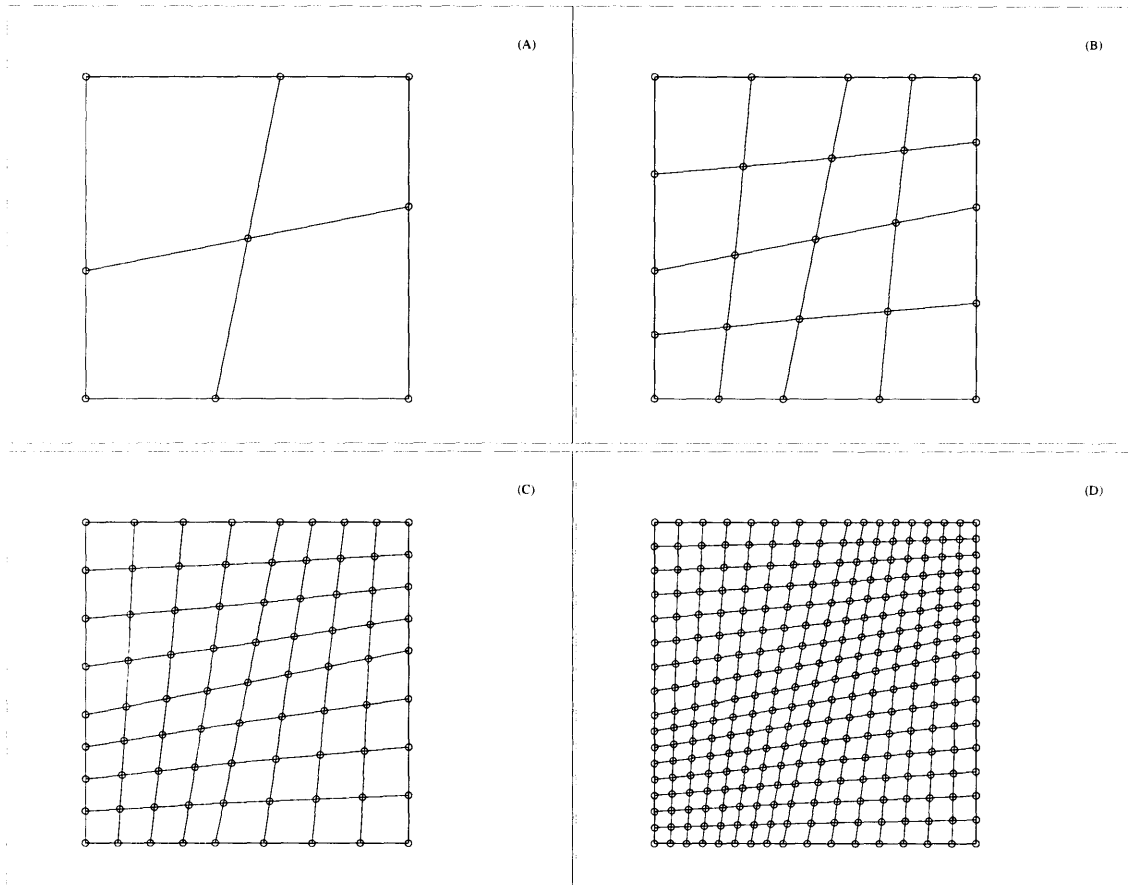


Figure 4-9: Distorted meshes used for the inf-sup test of the clamped plate problem.

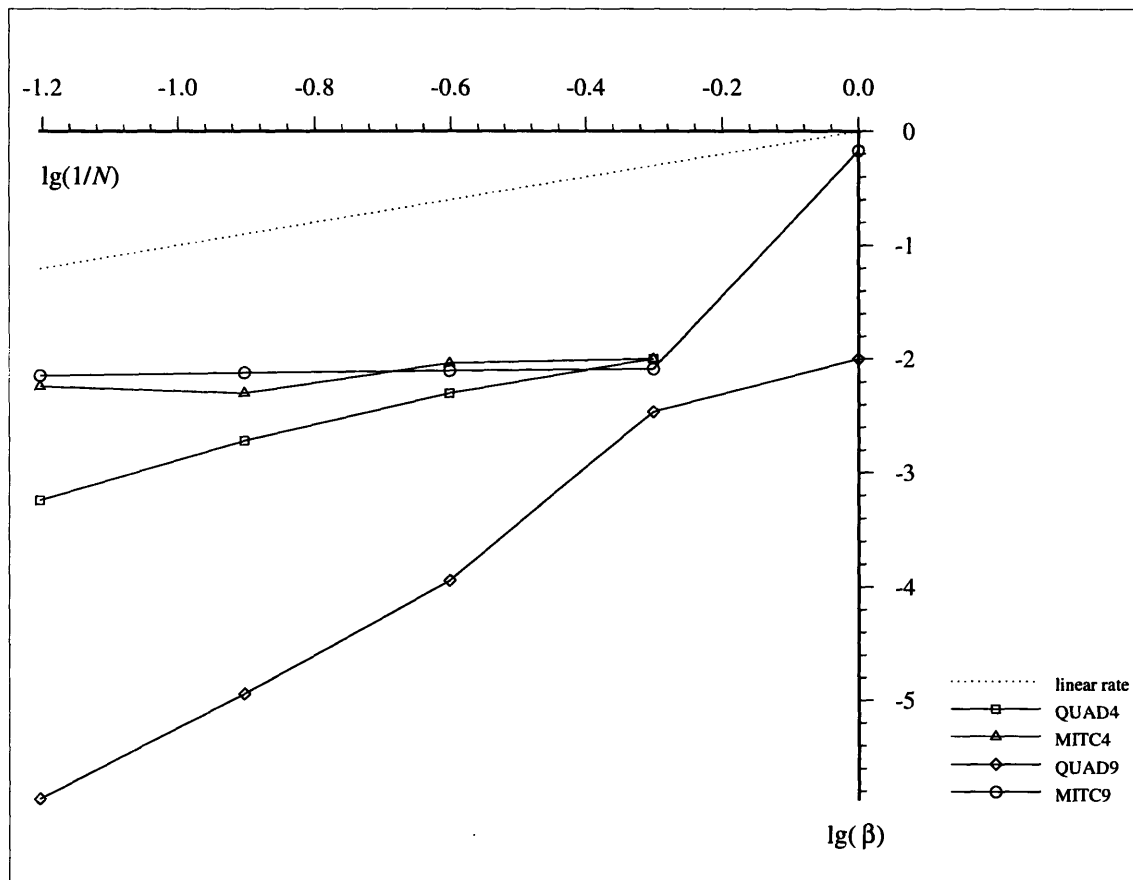


Figure 4-10: Inf-sup test of the quadrilateral plate bending elements in the Γ'_h -norm (clamped plate, distorted meshes).

Chapter 5

Conclusions.

The main objective of this thesis was to develop a reliable numerical testing procedure, which would indicate whether a particular element satisfies the inf-sup condition for a given discretization. This methodology was established, based on analytical results manifested in Chapters 2 and 3, using eigenvalue decompositions in a way similar to the inf-sup test proposed in [20]. All our predictions about the tested elements are in perfect agreement with analytical results, and with existing practical evidence (some results of numerical simulations are presented in Appendix A).

Moreover, Chapter 4 presents the essential apparatus, which can be applied to the numerical analysis of any constrained optimization problem, in which conditions of the inf-sup kind appear. Basically, the results can be generalized to any discrete functional, in particular, the extensions to nonlinear analysis and/or shell elements would be of great practical importance.

Summarizing the results of the analysis of the finite element discretizations for plate bending problems, we report that:

- (a) The four-node displacement-based element fails to satisfy the inf-sup condition, and thus should be excluded for practical use.
- (b) The nine-node displacement-based element passed the tests for uniform meshes,

but failed to work for reasonably distorted meshes; therefore this element should not be used for the analysis of complex geometries and in general nonlinear analysis. This finding explicitly emphasizes the importance of tests for meshes with distorted elements.

- (c) Elements of the MITC family (including the four-node MITC4 element) passed all tests including the tests using reasonably distorted meshes. Thus we predict that the elements satisfy the inf-sup condition, and therefore are reliable and effective elements to use in engineering analysis.

Appendix A

Shear locking.

Our purpose in this appendix is to present a number of numerical results which demonstrates shear locking phenomenon in plate bending problems.

A.1 Cantilever plate under a uniform load.

The first model problem is shown in the Fig. A-1 (top view is the same as in Fig. 4-1). The simplicity of the problem allows us to use beam theory (see e.g., [49])

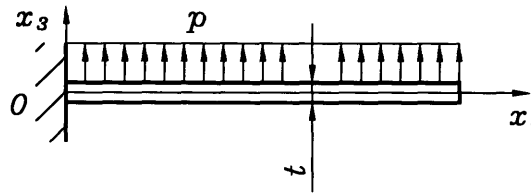


Figure A-1: Cantilever plate under a uniform load.

| t/L | QUAD4 | MITC4 | TRI7 | MITC7 | QUAD9 | MITC9 |
|--------|-------|-------|------|-------|-------|-------|
| 1/10 | 71.5 | 0.8 | 17.5 | 0.5 | 0.8 | 0.8 |
| 1/100 | 99.1 | 0.0 | 32.7 | 0.3 | 2.1 | 0.0 |
| 1/1000 | 99.9 | 0.0 | 33.3 | 0.3 | 2.1 | 0.0 |

Table A.1: Comparison of elements' performance in the norm $\|w_h\|$ (cantilever plate).

to obtain a good approximation for the exact solution.

$$w = pB \left[\frac{L^2}{4EI_2} x_1^2 - \frac{L}{6EI_2} x_1^3 + \frac{1}{24EI_2} x_1^4 \right], \quad I_2 = \frac{Bt^3}{12},$$

$$\theta_1 = 0,$$

$$\theta_2 = -pB \left[\frac{L^2}{2EI_2} x_1 - \frac{L}{2EI_2} x_1^2 + \frac{1}{6EI_2} x_1^3 \right],$$

$$\sigma_{11}^{\max} = \frac{M_2}{W_2}, \quad M_2 = \frac{1}{2} pB (L - x_1)^2, \quad W_2 = \frac{Bt^2}{6},$$

$$\sigma_{12} = 0,$$

$$\sigma_{13}^{\max} = \frac{3}{2} \frac{Q_3}{Bt}, \quad Q_3 = pB (L - x_1).$$

To check the performance of elements, we introduce a norm

$$\|w_h\| = \left| \frac{w_h(L) - w_{\max}}{w_{\max}} \right| \times 100\%, \quad (\text{A.1})$$

where $w_{\max} = w(L) = \frac{1}{8} \frac{pBL^4}{EI_2}$ and consider a sequence of plate's thicknesses, determined by the ratio t/L . Results of this test for a four-element mesh of four-, seven-, and nine-node displacement-based and MITC elements are shown in Table A.1.

The four-node displacement-based element produces results that correspond to the definition of locking – for small thicknesses displacements are almost zero. This can be easily explained by the fact that for the applied boundary con-

ditions, $Ker(B_\gamma) \equiv \underline{0}$, and therefore the interpolation space does not contain any functions satisfying the Kirchhoff constraint. Results of numerical simula-

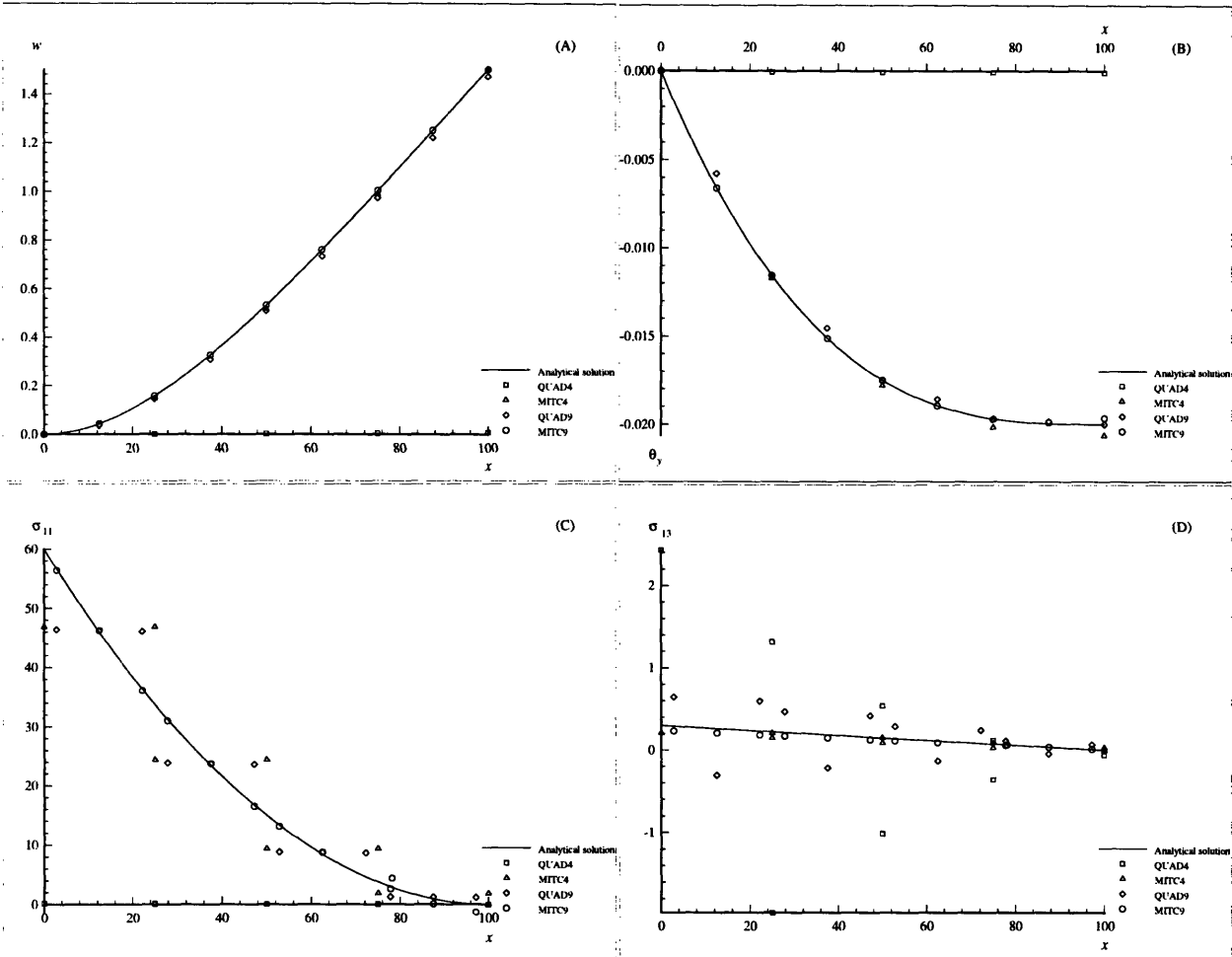


Figure A-2: Finite element solution (four-element meshes) for the cantilever plate case. (A) - transverse displacement w , mm; (B) - rotation angle θ_y ; (C) - normal stress σ_{11} , MPa; (D) - shear stress σ_{13} , MPa.

tions are presented in the Fig. A-2 for the case $L = B = 100$ mm, $t = 1$ mm, $E = 2 \cdot 10^5$ MPa, $\nu = 0$, $k = 5/6$, and $p = 2 \cdot 10^{-3}$ MPa.

A.2 Clamped square plate under a uniform load.

Let us now consider a thin square plate with all edges clamped, loaded by a uniform pressure p (see Fig. A-3; top view is the same as in Fig. 4-5). To

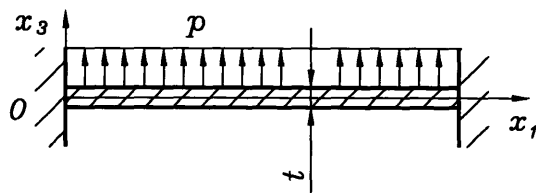


Figure A-3: Clamped plate under a uniform load.

compare the results of numerical simulations with theoretical predictions, we assume that the plate is thin enough for the Kirchhoff theory to provide a good approximation for the exact solution. Then, given the Poisson ratio $\nu = 0.3$, the maximal transverse displacement can be found as (see Section 44 of [48]):

$$w_{\max} = w\left(\frac{L}{2}; 0\right) = 0.00126 \frac{pL^4}{D}. \quad (\text{A.2})$$

Using w_{\max} as given above, we can compare the performance of elements in the norm (A.1). For the first comparative test we choose uniform meshes as shown in Fig. 4-6. The geometry and material characteristics are taken to be: $B = L = 100 \text{ mm}$, $E = 2 \cdot 10^5 \text{ MPa}$, $\nu = 0.3$, $k = 5/6$. The results of the test for different meshes and t/L -ratios are summarized in tables A.2 and A.3.

As in the first problem, the QUAD4 element locks, giving almost zero displacements for small thicknesses; moreover the chosen boundary conditions made the null space of B_γ -operator very small for the QUAD9 element, which resulted in significant deviations from the exact solution. The mixed-interpolated elements performed well, remaining robust to changes in thickness.

Fig. A-4 shows the numerical results for the transverse displacement $w(x_1, x_2)$ for the case $L = 100 \text{ mm}$, $t = 0.01 \text{ mm}$, $E = 2 \cdot 10^5 \text{ MPa}$, $\nu = 0.3$, $k = 5/6$,

| t/L | QUAD4 | MITC4 | QUAD9 | MITC9 |
|-----------|--------------|--------------|--------------|--------------|
| 1/10 | 8.6 | 18.1 | 14.3 | 20.6 |
| 1/100 | 97.1 | 0.5 | 20.8 | 2.1 |
| 1/1000 | 99.9 | 0.7 | 21.6 | 1.9 |
| 1/10,000 | 99.9 | 0.7 | 21.6 | 1.9 |
| 1/100,000 | 99.9 | 0.7 | 21.6 | 1.9 |

Table A.2: Comparison of elements' performance in the norm $\|w_h\|$ (clamped plate case, uniform meshes, 8×8 meshes for four-node elements, 4×4 meshes for nine-node elements).

| t/L | QUAD4 | MITC4 | QUAD9 | MITC9 |
|-----------|--------------|--------------|--------------|--------------|
| 1/10 | 11.1 | 19.1 | 19.0 | 19.5 |
| 1/100 | 97.2 | 0.2 | 4.4 | 0.7 |
| 1/1000 | 99.9 | 0.2 | 5.1 | 0.5 |
| 1/10,000 | 99.9 | 0.2 | 5.1 | 0.5 |
| 1/100,000 | 99.9 | 0.2 | 5.1 | 0.5 |

Table A.3: Comparison of elements' performance in the norm $\|w_h\|$ (clamped plate case, uniform meshes, 16×16 meshes for four-node elements, 8×8 meshes for nine-node elements).

and $p = 1.454 \cdot 10^{-7} MPa$ for the eight-by-eight mesh for four-node elements and four-by-four mesh for nine-node elements (the Kirchhoff theory solution is: $w_{\max} = 1 mm$).

Now for the same geometry and material, instead of taking uniform meshes, we will use slightly distorted discretizations. Thus, we pick a sequence of distorted meshes as shown in Fig. 4-9. The results of the runs for different mesh densities and t/L -ratios are shown in tables A.4, A.5.

| t/L | QUAD4 | MITC4 | QUAD9 | MITC9 |
|-----------|--------------|--------------|--------------|--------------|
| 1/10 | 11.1 | 18.2 | 13.5 | 20.9 |
| 1/100 | 97.2 | 0.5 | 24.5 | 2.5 |
| 1/1000 | 99.9 | 0.7 | 32.6 | 2.3 |
| 1/10,000 | 99.9 | 0.7 | 93.5 | 2.3 |
| 1/100,000 | 99.9 | 0.7 | 99.9 | 2.3 |

Table A.4: Comparison of elements' performance in the norm $\|w_h\|$ (clamped plate case, distorted meshes, 8×8 meshes for four-node elements, 4×4 meshes for nine-node elements).

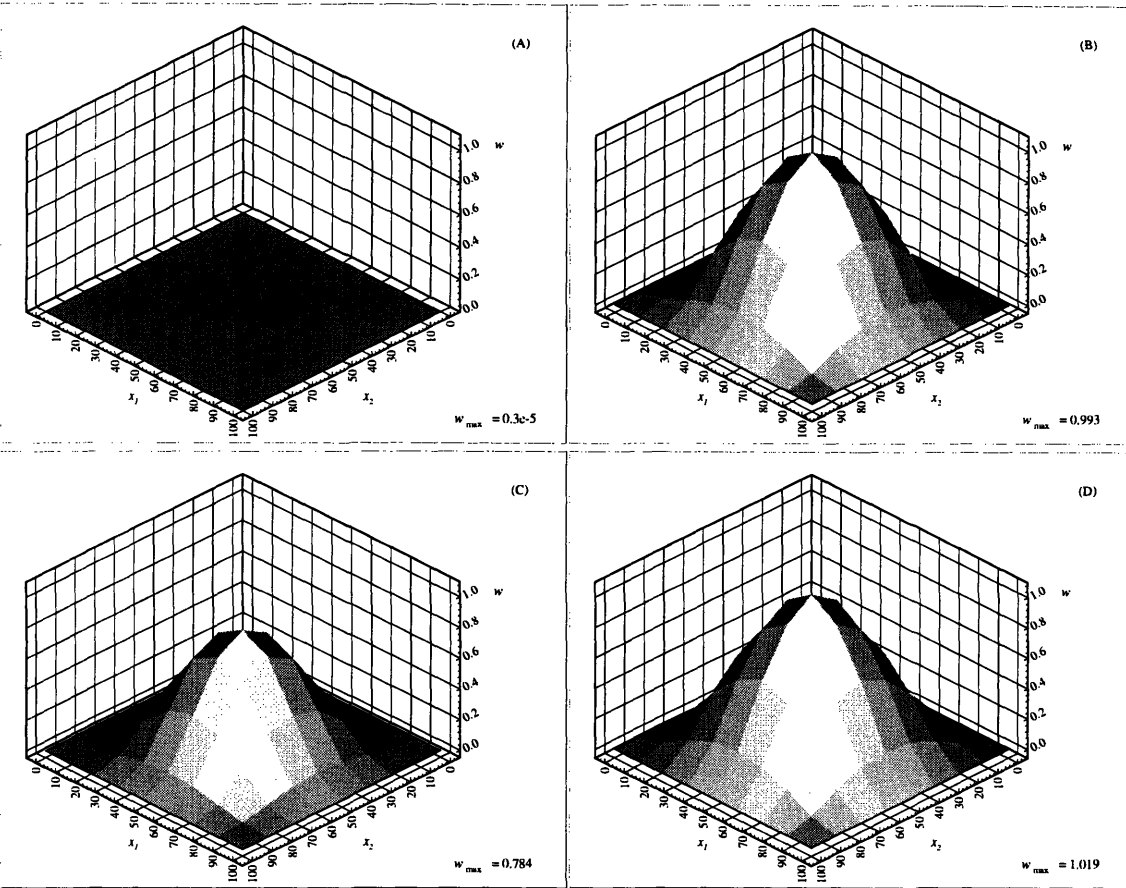


Figure A-4: FE solution for the transverse displacement w , mm , (8-by-8 uniform meshes for 4-node elements, 4-by-4 meshes for 9-node elements) for the clamped plate case. (A) - QUAD4 element; (B) - MITC4 element; (C) - QUAD9 element; and (D) - MITC9 element.

Clearly, one can see that the QUAD9's behavior changed drastically – it is no longer robust to changes in thickness, and locks for small t/L ratios. Fig. A-5 demonstrates qualitative changes (when compared with Fig. A-4) in the calculated transverse displacement w for the four elements. While displacement-based elements failed to work, the MITC4 and MITC9 elements show robustness to mesh distortions, and reliable anti-locking properties.

| t/L | QUAD4 | MITC4 | QUAD9 | MITC9 |
|-----------|-------|-------|-------|-------|
| 1/10 | 9.7 | 19.3 | 18.9 | 19.5 |
| 1/100 | 89.9 | 0.4 | 5.1 | 0.7 |
| 1/1000 | 99.9 | 0.2 | 6.3 | 0.5 |
| 1/10,000 | 99.9 | 0.2 | 31.0 | 0.5 |
| 1/100,000 | 99.9 | 0.2 | 97.2 | 0.5 |

Table A.5: Comparison of elements' performance in the norm $\|w_h\|$ (clamped plate case, distorted meshes, 16×16 meshes for four-node elements, 8×8 meshes for nine-node elements).

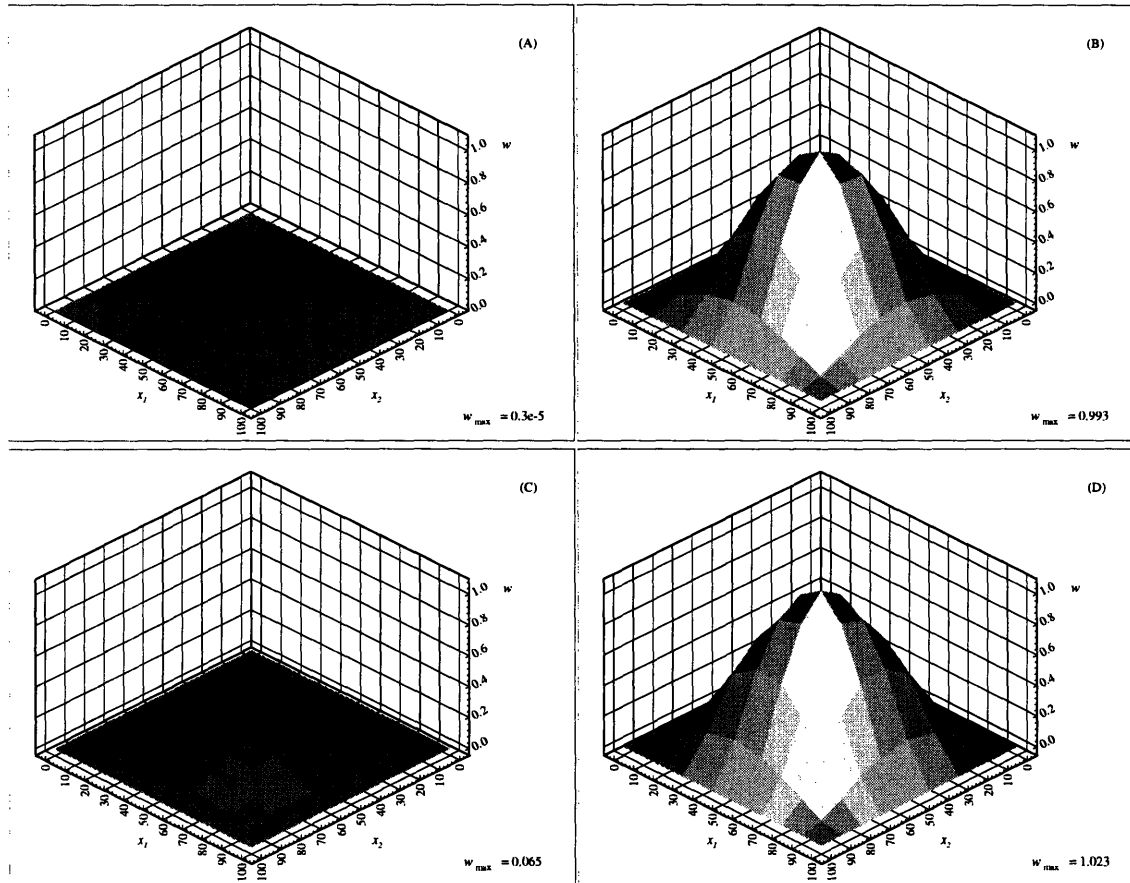


Figure A-5: FE solution for the transverse displacement w , mm , (8 -by- 8 distorted meshes for 4 -node elements, 4 -by- 4 meshes for 9 -node elements) for the clamped plate. (A) - QUAD4 element; (B) - MITC4 element; (C) - QUAD9 element; and (D) - MITC9 element.

Appendix B

Inf-sup test in the Γ'_h -norm.

This appendix presents an alternative derivation of the numerical inf-sup test, described in Section 4.2.3.

Following the notation of Section 4.2, we will find the inf-sup value β as

$$\inf_{\mathbf{U} \in \mathcal{D}} \sup_{\mathbf{V} \in \mathcal{D}} \frac{\mathbf{U}^T \mathbf{G} \mathbf{V}}{\sup_{\mathbf{W} \in \mathcal{D}} \frac{\mathbf{W}^T \mathbf{G} \mathbf{U}}{|\mathbf{W}|_{\mathbf{D}}} \|\mathbf{V}\|_{\mathbf{S}}} \geq \beta \quad (\text{B.1})$$

By (4.5) we have:

$$|\mathbf{W}|_{\mathbf{D}} \geq \sqrt{\delta_{\min}} \|\mathbf{W}\|_2,$$

and thus

$$\sup_{\mathbf{W} \in \mathcal{D}} \frac{\mathbf{W}^T \mathbf{G} \mathbf{U}}{|\mathbf{W}|_{\mathbf{D}}} \leq \frac{1}{\sqrt{\delta_{\min}}} \sup_{\mathbf{W} \in \mathcal{D}} \frac{\mathbf{W}^T \mathbf{G} \mathbf{U}}{\|\mathbf{W}\|_2} \stackrel{\text{use (4.6)}}{=} \frac{1}{\sqrt{\delta_{\min}}} \|\mathbf{G} \mathbf{U}\|_2 \quad (\text{B.2})$$

Now we rewrite $\mathbf{V} = \Phi \widetilde{\mathbf{V}}$, $\mathbf{U} = \Phi \widetilde{\mathbf{U}}$, where $\Phi = \{\underline{\phi}_1, \dots, \underline{\phi}_n\}$ is the set of \mathbf{S} -orthonormal eigenvectors of the $GEP(\mathbf{G}, \mathbf{S})$; let $\Lambda = \text{diag}(\lambda_1, \dots, \lambda_n)$ be the

corresponding eigenvalue matrix; then

$$\begin{aligned}
\sup_{\mathbf{V} \in \mathcal{D}} \frac{\mathbf{U}^T \mathbf{G} \mathbf{V}}{\|\mathbf{V}\|_{\mathbf{S}}} &= \sup_{\Phi \tilde{\mathbf{V}} \in \mathcal{D}} \frac{\tilde{\mathbf{U}}^T \Phi^T \mathbf{G} \Phi \tilde{\mathbf{V}}}{\|\Phi \tilde{\mathbf{V}}\|_{\mathbf{S}}} = \\
&= \sup_{\Phi \tilde{\mathbf{V}} \in \mathcal{D}} \frac{\tilde{\mathbf{U}}^T \Lambda \tilde{\mathbf{V}}}{\|\tilde{\mathbf{V}}\|_2} \stackrel{\text{use (4.6)}}{=} \frac{\|\Lambda \tilde{\mathbf{U}}\|_2 \|\tilde{\mathbf{V}}\|_2}{\|\tilde{\mathbf{V}}\|_2} = \\
&= \|\Lambda \Phi^{-1} \mathbf{U}\|_2 \stackrel{\text{use } \Phi^T \mathbf{G} \Phi = \Lambda}{=} \|\Phi^T \mathbf{G} \mathbf{U}\|_2 \geq \sqrt{\vartheta_{\min}} \|\mathbf{G} \mathbf{U}\|_2,
\end{aligned} \tag{B.3}$$

where $\sqrt{\vartheta_{\min}}$ is the smallest eigenvalue of the matrix $\Theta = \Phi \Phi^T$.

Substituting results of (B.3) and (B.2) into (B.1), we obtain

$$\inf_{\mathbf{U} \in \mathcal{D}} \sup_{\mathbf{V} \in \mathcal{D}} \frac{\mathbf{U}^T \mathbf{G} \mathbf{V}}{\|\mathbf{B}_\gamma \mathbf{U}\|_{\Gamma'_h} \|\mathbf{V}\|_{\mathbf{S}}} \geq \sqrt{\delta_{\min}} \sqrt{\vartheta_{\min}} \inf_{\mathbf{U} \in \mathcal{D}} \frac{\|\mathbf{G} \mathbf{U}\|_2}{\|\mathbf{G} \mathbf{U}\|_2} \stackrel{\text{use } \mathbf{U} \in \mathcal{D}}{=} \sqrt{\delta_{\min}} \sqrt{\vartheta_{\min}} = \beta. \tag{B.4}$$

Note that to obtain ϑ_{\min} we have to calculate the full set of eigenvectors Φ , and then run the eigensolver for a full matrix Θ , which is a relatively expensive scheme. From computational point of view, the procedure of Section 4.2.3 is much cheaper and far more stable.

Let us finally point out that the two methods produce absolutely the same numerical results, and therefore they can be viewed as the perfect substitutes from the analytical point of view.

Bibliography

- [1] D.A. Adams. *Sobolev Spaces*. Academic Press, New York, 1975.
- [2] I. Babuška. The finite element method with Lagrange multipliers. *Num. Math.*, 20:179-192, 1973.
- [3] I. Babuška, L. Li. The problem of plate modeling: Theoretical and computational results. *Comp. Meth. in Appl. Mech. and Engrg.*, 100:249-273, 1992.
- [4] I. Babuška, M. Suri. The p and h - p versions of the finite element method, basic principles and properties. *SIAM Review*, Vol. 36, 4:578-632, 1994.
- [5] S. Banach. *Theory of linear operators*. North-Holland, 1987.
- [6] K.J. Bathe. *Finite Element Procedures*. Prentice Hall, Englewood Cliffs, 1996.
- [7] K.J. Bathe, F. Brezzi. On the convergence of a four-node plate bending element based on Mindlin/Reissner plate theory and a mixed interpolation. *The Mathematics of Finite Elements and Applications V*, Academic Press Inc., 491-503, 1985.
- [8] K.J. Bathe, F. Brezzi. A simplified analysis of two plate bending elements – the MITC4 and MITC9 elements. *Proceedings, Numerical Methods in Engineering: Theory and Applications*, University College, Swansea, U.K., 1987.

- [9] K.J. Bathe, M.L. Bucalem, F. Brezzi. Displacement and stress convergence of our MITC plate bending elements. *Engrg. Comp.*, 7:291-302, 1990.
- [10] K.J. Bathe, E.N. Dvorkin. A four-node plate bending element based on Mindlin/Reissner plate theory and a mixed interpolation. *Int. J. Num. Meth. in Engrg.*, 21:367-383, 1985.
- [11] G.P. Bazeley, Y.K. Cheung, B.M. Irons, O.C. Zienkiewicz. Triangular elements in plate bending – conforming and non-conforming solutions. *Proc. 1st Conf. on Matrix Meth. in Struct. Mech.*, 547-576, 1965.
- [12] F.K. Bogner, R.L. Fox, L.A. Schmit, Jr. The generation of inter-element compatible stiffness and mass matrices by use of interpolation formulas. *Proc. 1st Conf. on Matrix Meth. in Struct. Mech.*, 397-443, 1965.
- [13] F. Brezzi. On the existence, uniqueness and approximation of saddle-point problems arising from Lagrangian multipliers. *RAIRO*, R-2:129-151, 1974.
- [14] F. Brezzi, K.J. Bathe. A discourse on the stability conditions for mixed finite element formulations. *Comp. Meth. in Appl. Mech. and Engrg.*, 82:27-57, 1990.
- [15] F. Brezzi, K.J. Bathe, M. Fortin. Mixed-interpolated elements for Reissner-Mindlin plates. *Int. J. Num. Meth. in Engrg.*, 28:1787-1801, 1989.
- [16] F. Brezzi, J. Douglas, R. Duran, M. Fortin. Mixed finite elements for second order elliptic problems in three variables. *Num. Math.*, 51:237-250, 1987.
- [17] F. Brezzi, J. Douglas, M. Fortin, L.D. Marini. Efficient rectangular mixed finite elements in two and three space variables. *Math. Model. Num. Anal.*, 21:581-604, 1987.
- [18] F. Brezzi, M. Fortin. *Mixed and Hybrid Finite Element Methods*. Springer-Verlag, 1991.

- [19] F. Brezzi, M. Fortin, R. Stenberg. Error analysis of mixed-interpolated elements for Reissner-Mindlin plates. *Math. Models and Methods in Appl. Sciences*, Vol. 1, 2:125-151, 1991.
- [20] D. Chapelle, K.J. Bathe. The inf-sup test. *Computers & Structures*, Vol. 47, 4/5:537-545, 1993.
- [21] R.W. Clough, J.L. Tocher. Finite element stiffness matrices for the analysis of plate bending. *Proc. 1st Conf. on Matrix Meth. in Struct. Mech.*, 515-545, 1965.
- [22] P.G. Ciarlet. *The Finite Element Method for Elliptic Problems*. North-Holland, Amsterdam, 1978.
- [23] P.G. Ciarlet, P. Destuynder. A justification of the two-dimensional linear plate model. *J. Mécanique*, 12:315-344, 1979.
- [24] E.N. Dvorkin, K.J. Bathe. A continuum mechanics based four-node shell element for general nonlinear analysis. *Engrg. Comp.*, 1:77-88, 1984.
- [25] G. Golub, C.F. Van Loan. *Matrix Computations*. John Hopkins, 1989.
- [26] B. Häggblad, K.J. Bathe. Specifications of boundary conditions for Reissner-Mindlin plate bending finite elements. *Int. J. Num. Meth. Engrg.*, 30:981-1011, 1990.
- [27] M.M. Hrabok, T.M. Hrudey. A review and catalogue of plate bending finite elements. *Computers & Structures*, Vol. 19, 3:479-495, 1984.
- [28] H.C. Hu. On some variational principles in the theory of elasticity and the theory of plasticity. *Scientia Sinica*, 4:33-54, 1955.
- [29] T.J.R. Hughes, R.L. Taylor, W. Kanoknukulchai. A simple and efficient finite element for plate bending. *Int. J. Num. Meth. Engrg.*, 11:1529-1543, 1977.

- [30] O.K. Jain, V.P. Gupta. *Lebesgue Measure and Integration*, John Wiley & Sons, 1986.
- [31] D.D. Jensen, K.C. Park. Equilibrium constrained assumed natural coordinate strain plate elements. *Int. J. Num. Meth. Engrg.*, 38:2951-2977, 1995.
- [32] C. Johnson, J. Pitkäranta. Analysis of some mixed finite element methods related to reduced integration. *Math. Comp.*, 38:375-400, 1982.
- [33] O.A. Ladyzhenskaya. *The Mathematical Theory of Viscous Incompressible Flow*. Gordon and Breach, 1969.
- [34] D.S. Malkus. Eigenproblems associated with the discrete LBB condition for incompressible finite elements. *Int. J. Engrg. Sci.*, 19:1299:1310, 1981.
- [35] D.S. Malkus, T.J.R. Hughes. Mixed finite element methods - reduced and selective integration techniques: a unification of concepts. *Comp. Meth. in Appl. Mech. and Engrg.*, 15:63-81, 1978
- [36] R.D. Mindlin. Influence of rotatory inertia and shear on flexural motions of isotropic, elastic plates. *J. Appl. Mech.*, 18:31-38, 1951.
- [37] L.S.D. Morley. A triangular element with linearly varying bending moments for plate bending problems. *The Aeronaut. J. Royal Aeronaut. Soc.*, 71:715-719, 1967.
- [38] J.T. Oden. *Applied Functional Analysis. A First Course for Students of Mechanics and Engineering Science*. Prentice-Hall, Englewood Cliffs, 1979.
- [39] S.F. Pawsey, R.W. Clough. Improved numerical integration of thick shell finite elements. *Int. J. Num. Meth. Engrg.*, 3:575-586, 1971.
- [40] T.H.H. Pian, P. Tong. Basis of finite element methods for solid continua. *Int. J. Num. Meth. Engrg.*, 1:3-28, 1969.

- [41] J. Pitkäranta, M. Suri. Design principles and error analysis for reduced-shear plate-bending finite elements. To appear in *Num. Math.*, 1997.
- [42] P.A. Raviart, J.M. Thomas. A mixed finite element method for second order elliptic problems. *Math. Aspects of the Finite Element Method* (I. Galligani, E. Magenes, eds.), Lecture Notes in Math. 606, Springer-Verlag, 1977.
- [43] E. Reissner. The effect of transverse shear deformation on the bending of elastic plates. *J. Appl. Mech.*, 67:A69-A77, 1945.
- [44] C. Schwab, M. Suri. Locking and boundary layer effects in the finite element approximation of the Reissner-Mindlin plate model. *Proceedings Symp. Appl. Math.*, 48:367-371, AMS, Providence, 1994.
- [45] R. Stenberg, M. Suri. An hp analysis of MITC plate elements. To appear in *SIAM J. Num. Analysis*, 1996.
- [46] G. Strang, G.J. Fix. *An Analysis of the Finite Element Method*. Prentice-Hall, Englewood Cliffs, 1973.
- [47] M. Suri, I. Babuška, and C. Schwab. Locking effects in the finite element approximation of plate models. *Math. Comp.*, 64:461:482, 1995.
- [48] S.P. Timoshenko, S. Woinowsky-Krieger. *Theory of Plates and Shells*. McGraw-Hill, Inc., 1995.
- [49] S.P. Timoshenko. *Strength of Materials*. Van Nostrand, 1956.
- [50] P. Tong. New displacement hybrid finite element models for solid continua. *Int. J. Num. Meth. Engrg.*, 2:73-83, 1970.
- [51] B. Fraeijis de Veubeke, O.C. Zienkiewicz. Strain energy bounds in finite element analysis by slab analogy. *J. Strain Analysis*, 2:265-271, 1967.
- [52] K. Yosida. *Functional Analysis*. Springer-Verlag, 1971.

- [53] O.C. Zienkiewicz, R.L. Taylor, J.M. Too. Reduced integration technique in general analysis of plates and shells. *Int. J. Num. Meth. Engrg.*, 3:275-290, 1971.